International Journal of Coal Geology 226 (2020) 103499

Contents lists available at ScienceDirect

International Journal of Coal Geology

journal homepage: www.elsevier.com/locate/coal

# Frictional properties of simulated shale-coal fault gouges: Implications for induced seismicity in source rocks below Europe's largest gas field

Jinfeng Liu[a,b,c,*], Luuk B. Hunfeld[d], André R. Niemeijer[d], Christopher J. Spiers[d]

[a] School of Earth Sciences and Engineering, Sun Yat-Sen University, 510275 Guangzhou, China
[b] Guangdong Provincial Key Lab of Geodynamics and Geohazards, Sun Yat-Sen University, Zhuhai, China
[c] Southern Marine Science and Engineering Guangdong Laboratory, Zhuhai, China
[d] Department of Earth Sciences, Utrecht University, 3584, CB, Utrecht, The Netherlands

ARTICLE INFO

*Keywords:*
Slip-weakening
Rate-and-state friction
Frictional healing
Coal-rich shear bands
Pore fluids effects
Groningen Carboniferous

ABSTRACT

We report 21 frictional sliding experiments performed on simulated fault gouges prepared from shale-coal mixtures. Our aim was to investigate the effects of local coal seam smearing on the frictional properties and induced seismogenic potential of faults cutting the Upper Carboniferous source rocks underlying the Groningen gas reservoir (Netherlands). We used shale/siltstone core recovered from beneath the Groningen reservoir plus Polish bituminous coal of similar age and origin to coals locally present in the Groningen source rocks. We performed friction experiments in velocity stepping, constant velocity, slide-hold-slide (SHS) and slide-unload-slide (SUS) modes, under near in-situ conditions of 100 °C and 40 MPa effective normal stress, employing sliding velocities of 0.1–100 μm/s and a variety of pore fluids. Samples with 0–50 vol% coal showed friction coefficients ~0.45, with minor slip weakening. Samples with ≥50 vol% coal showed marked slip-weakening from peak friction values of ~0.47 to ~0.3, regardless of experimental conditions, presumably reflecting strain localization in weak coal-rich shear bands, possibly accompanied by changes in coal molecular structure. However, re-sliding experiments (SUS) showed that slip-weakening is limited to small initial displacements (2–3 mm), and does not occur during slip reactivation. At (near) steady state, almost all experiments performed at in-situ stress, pore water pressure (15 MPa) and temperature conditions exhibited stable, velocity strengthening behaviour, regardless of coal content. By contrast, under dry and gas-saturated ($CH_4$, Argon) conditions, or using water at 1 atm, 50:50 (vol%) shale-coal mixtures showed velocity-weakening and even stick-slip. Our results imply that faults in the Groningen Carboniferous shale-siltstone sequence are not prone to induced earthquake nucleation at in-situ conditions, even when coal-bearing or coal-enriched by smearing. However, the mechanisms controlling coal friction remain unclear at the sliding velocities studied, and the evolution of coal friction at seismic slip velocities remains unknown.

## 1. Introduction

Induced seismicity caused by natural gas and oil recovery (e.g. Van Eijs et al., 2006), mining (Cook, 1976; Westbrook et al., 1980), water injection (Ellsworth, 2013; Guglielmi et al., 2015), and geothermal energy production (e.g. Majer et al., 2007), has increased globally in recent years. Many studies have attempted to understand induced seismicity in shale and conventional gas fields, from different perspectives (Ellsworth, 2013; Elsworth et al., 2016; Guglielmi et al., 2015; Hunfeld et al., 2017). However, data on the frictional properties of field-specific fault and reservoir rocks under in-situ stress-pressure-temperature conditions remain limited. These are key to a better understanding and better modelling of the seismic vs. aseismic response of faults to changes in stress-state associated with pore pressure changes due to production or mining or injection.

In this contribution, we address induced seismicity in the Groningen gas field of the N.E. Netherlands. This is one of the largest single onshore gas fields in the world and the largest in Europe. A stratigraphic column showing the main formations in the field is presented in Fig. 1. It consists of 1) the Carboniferous shale/siltstone substrate which includes Westphalian coal seams and kerogen-bearing shale source rocks (De Jager and Visser, 2017), 2) the unconformably overlying Upper Rotliegend, Slochteren sandstone reservoir rock, 3) the Ten Boer claystone, and 4) the Basal Zechstein anhydrite-carbonate evaporite caprock. In the last few decades, the Groningen gas field has shown substantial production-induced seismicity, long thought to be caused by

* Corresponding author at: School of Earth Sciences and Engineering, Sun Yat-Sen University, 510275 Guangzhou, China.
*E-mail address:* liujinf5@mail.sysu.edu.cn (J. Liu).

https://doi.org/10.1016/j.coal.2020.103499
Received 29 November 2019; Received in revised form 29 April 2020; Accepted 30 April 2020
Available online 05 May 2020
0166-5162/ 

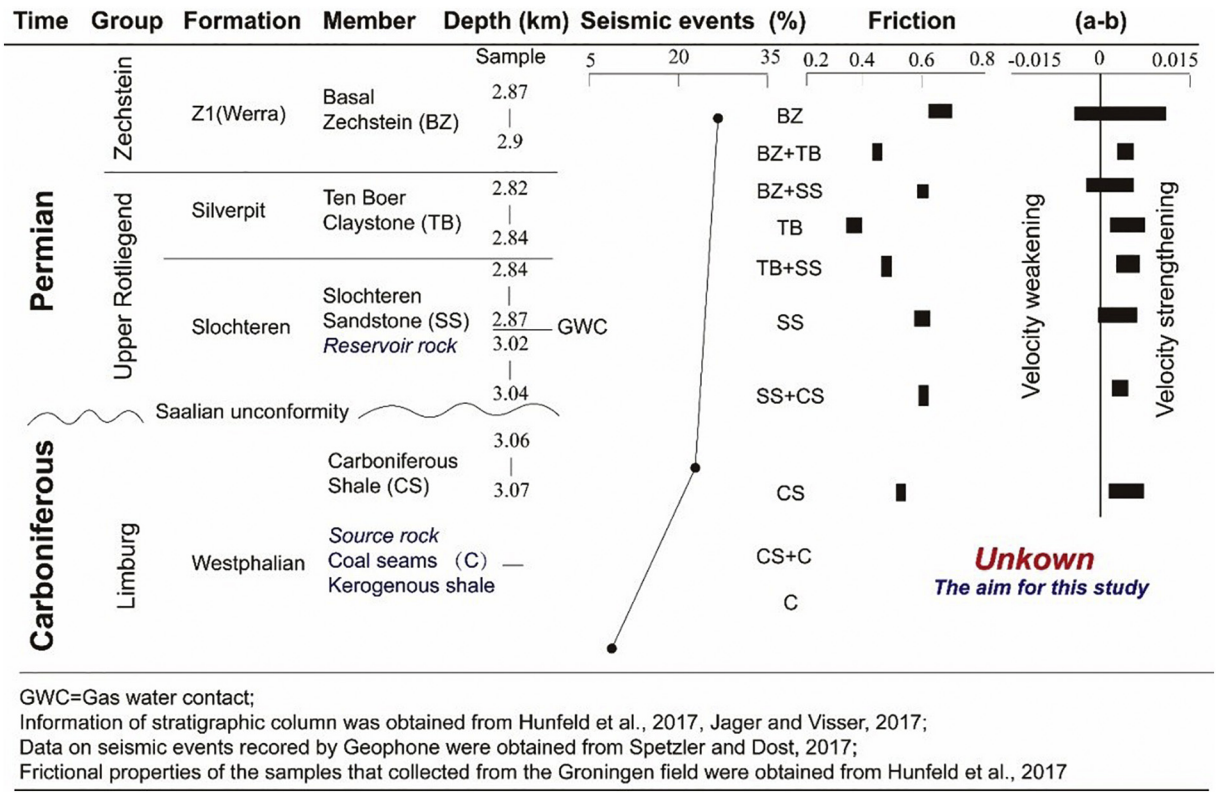


**Fig. 1.** Schematic illustration of stratigraphic column, seismic events recorded by geophone, and the frictional properties [frictional coefficient and its velocity dependence expressed in the parameter (a–b)] of simulated fault gouge samples from the Groningen field, as determined by Hunfeld et al. (2017). "Unknown" indicates the aim of the present study of determining frictional coefficient and (a–b) in simulated coal-bearing Carboniferous gouges.

reactivation of the many, pre-existing normal faults that cut the reservoir and surrounding units (NAM, 2013; Van Eijs et al., 2006). Since 2015, improvements in geophone density and seismic event locations have confirmed a spatial correlation with the main fault sets present in the field (Spetzler and Dost, 2017). In addition, recent geomechanical modelling studies of the Groningen situation (Buijze et al., 2017, 2019) have shown that gas pressure reduction leads to an increase in shear stress and a decrease in effective normal stress on pre-existing normal faults that offset the reservoir, causing fault reactivation within and close to the reservoir when the frictional strength is attained – as well as unstable rupture if subsequent fault weakening is allowed. Data on the frictional behaviour of fault rocks derived from the relevant formations, under the presently pertaining in-situ stress, pore fluid pressure, temperature and chemical conditions, are therefore needed a) for assessing the reservoir pressure and stress changes that can cause fault reactivation, and hence b) for assessing seismic hazard (Spiers et al., 2017; Van Eijs et al., 2006; Van Thienen-Visser and Breunese, 2015; Van Wees et al., 2014).

Hunfeld et al. (2017) performed a series of frictional sliding experiments on simulated fault gouges prepared from core and drill cuttings, identifying which formations within the Groningen reservoir system are most likely to exhibit seismic reactivation of cross-cutting, gouge-filled faults, in response to gas production. Following a Rate and State Dependent Friction (RSF) approach (Dieterich, 1978, 1979; Ruina, 1983), these authors obtained the frictional strength and rate-dependence of friction for samples collected from the formations illustrated in Fig. 1, under in-situ conditions and at low shearing (slip patch nucleation) velocities (0.1–10 μm/s). They observed a marked frictional stratigraphy whereby a) frictional strength was low in the phyllosilicate rich Ten Boer and Carboniferous but high in the reservoir and Basal Zechstein, and b) only the Basal Zechstein (and its mixtures with sandstone gouge) exhibited unstable, velocity-weakening RSF behaviour, depending strongly on pore fluid salinity, temperature and gas-brine pore saturation ratio. From the RSF perspective, widely used to evaluate the seismic potential of tectonically active faults, this implies that the most likely location for seismogenic slip nucleation may be on faults towards and just above the top of the reservoir, i.e. on fault segments containing Basal Zechstein-derived gouges, especially where these are dry (gas saturated) or relatively hot. This is consistent with the seismological observations reported by Spetzler and Dost (2017) that ~30% of seismic events occurred on faults in the Basal Zechstein with a skew in event frequency towards the reservoir top.

On the other hand, the geophone data reported by Spetzler and Dost (2017) also show that ~15% of earthquake events in Groningen gas field occurred below the reservoir unit, in the Carboniferous substrate. This is not explained by the experiments of Hunfeld et al. (2017), at least from an RSF viewpoint, as these demonstrate stable, velocity-strengthening behaviour of simulated Carboniferous gouges. Coincidentally, the Groningen Carboniferous core samples investigated by Hunfeld et al. (2017) contain no organic matter. Recently, graphitization of carbonaceous materials at rapid fault slip rates (> 10 mm/s), has been shown to lead to dynamic weakening (Kuo et al., 2014; Oohashi et al., 2011). This has raised the question of whether seismicity in the Carboniferous may reflect a destabilizing role of the thin coal seams and organic-rich shales that are known to be widely present (see Fig. 1; De Jager and Visser, 2017), potentially promoting seismic rupture propagation to unexpectedly large depths. It is unknown, however, whether the presence of coal can result in lubrication effects (i.e. decreasing friction) during shear deformation at low (rupture nucleation) velocities, as no data exist on the frictional properties of coal or shale-coal mixtures under reservoir conditions.

In this paper, we investigate whether the presence of coal has any effects on the frictional properties of Carboniferous shale/siltstone substrate material collected from the Groningen gas field. This was achieved by performing friction experiments on simulated fault gouge samples with varying coal content in volume fractions of 0–100 vol%,

**Table 1**
List of experiments, experimental conditions and key mechanical data.

| Exp./Sam. | Coal C [vol%] | Pore fluids | $P_f$ [MPa] | $\sigma_n$ [MPa] | $\mu_{peak}$ [−] | $\mu_{ss1}$ [−] | $\mu_{ss2}$ [−] | $D_{tot}$ [mm] | V [μm/s] | $t_0$ [mm] | t [mm] |
|---|---|---|---|---|---|---|---|---|---|---|---|
| VS | | | | | | | | | | | |
| VS_1 | 0 | $H_2O$ | 15 | 55 | 0.481 | 0.466 | 0.445 | 5.721 | 0.3–100 | 0.75 | 0.60 |
| VS_2 | 10 | $H_2O$ | 15 | 55 | 0.500 | 0.458 | 0.403 | 5.731 | 0.3–100 | 0.95 | 0.85 |
| VS_3 | 25 | $H_2O$ | 15 | 55 | 0.493 | 0.464 | 0.377 | 5.649 | 0.3–100 | 1.00 | 0.80 |
| VS_4 | 33 | $H_2O$ | 15 | 55 | 0.504 | 0.443 | 0.352 | 5.581 | 0.3–100 | 0.85 | 0.80 |
| VS_5 | 50 | $H_2O$ | 15 | 55 | 0.482 | 0.316 | 0.289 | 5.758 | 0.3–100 | 0.80 | 0.65 |
| VS_6 | 75 | $H_2O$ | 15 | 55 | 0.466 | 0.285 | 0.264 | 5.731 | 0.3–100 | 0.90 | 0.70 |
| VS_7 | 100 | $H_2O$ | 15 | 55 | 0.449 | 0.296 | 0.264 | 5.745 | 0.3–100 | 0.95 | 0.75 |
| VS_8 | 50 | Vacuum | 0 | 40 | 0.499 | 0.318 | 0.285 | 5.799 | 0.3–100 | 0.80 | 0.65 |
| VS_9 | 50 | Lab dry | 0.1 | 40 | 0.446 | 0.327 | 0.341 | 5.795 | 0.1–100 | 0.83 | 0.65 |
| VS_10 | 50 | $H_2O$ | 0.1 | 40 | 0.434 | 0.314 | 0.314 | 5.820 | 0.1–100 | 0.77 | 0.62? |
| VS_11 | 0 | $CH_4$ | 15 | 55 | 0.535 | 0.539 | 0.515 | 5.694 | 0.1–100 | 0.70 | 0.55 |
| VS_12 | 100 | $CH_4$ | 15 | 55 | 0.498 | 0.336 | 0.288 | 5.734 | 0.1–100 | 0.97 | 0.80 |
| VS_13 | 50 | $CH_4$ | 15 | 55 | 0.460 | 0.330 | 0.329 | 6.022 | 0.1–100 | 0.77 | 0.57 |
| VS_14 | 50 | Argon | 15 | 55 | 0.459 | 0.340 | 0.338 | 5.678 | 0.1–100 | 0.83 | 0.57 |
| CS | | | | | | | | | | | |
| CS_1 | 50 | $H_2O$ | 15 | 55 | 0.500 | 0.342 | | 2.845 | 0.1 | 0.85 | 0.75 |
| CS_2 | 50 | $H_2O$ | 15 | 55 | 0.449 | 0.341 | | 2.673 | 1 | 0.67 | 0.55 |
| CS_3 | 50 | $H_2O$ | 15 | 55 | 0.413 | 0.302 | | 2.704 | 10 | 0.87 | 0.62 |
| CS_4 | 50 | $H_2O$ | 15 | 55 | 0.383 | 0.284 | 0.298 | 5.480 | 100 | 0.73 | 0.55 |
| SHS | | | | | | | | | | | |
| SHS_1 | 50 | $H_2O$ | 15 | 55 | 0.460 | 0.347 | 0.309 | 5.384 | 1 | 0.90 | 0.65 |
| SUS | | | | | | | | | | | |
| SUS_1 | 50 | $H_2O$ | 15 | 55 | 0.424 | 0.325 | 0.328 | 3.564 | 1 | 0.95 | 0.85? |
| SUS_2 | 50 | $H_2O$ | 15 | 55 | 0.461 | 0.347 | 0.316 | 5.687 | 1 | 0.40 | 0.25 |

VS = velocity stepping, CS = constant velocity, SHS = Slide-hold-Slide and SUS = Slide-unload-slide tests. Note that all experiments reported here were performed at 100 °C. Coal content represents the volume fraction (%) composition of the coal-shale mixtures used to simulate mixed fault gouges. $P_f$ and $\sigma_n$ represent the pore fluid pressure and confining pressures employed in the experiments. $\mu_{peak}$ represents the peak friction coefficient obtained at 0.42–1.26 mm shear displacement, $\mu_{ss1}$ represents the steady-state friction coefficient obtained at ~2.2 mm shear displacement, and $\mu_{ss2}$ represents the steady-state friction coefficient obtained at ~5.7 mm shear displacement (near the end of each experiment). In the constant velocity experiments, $\mu_{ss1} \approx \mu_{ss2}$. $D_{tot}$ represents the total shear displacement. $t_0$ and $t$ represent the thickness of the gouge layer measured before and after the experiments, respectively.

using a conventional triaxial testing machine equipped with an internal direct shear sample assembly and external loading frame. The experiments were performed at nominally constant sliding (shearing) velocity (i.e. constant loading frame drive velocity), in some cases incrementally increasing or decreasing (stepping) the slip rate, or even holding and then restarting slip, to determine the effects of slip velocity and of static healing time on frictional strength. We applied near in-situ conditions of 100 °C and 40 MPa effective normal stress (Terzaghi definition), employing pore fluids ranging from water to methane and sliding velocities (imposed loading frame displacement rates) of 0.1–100 μm/s to simulate the onset of fault motion in a nucleating rupture patch. We followed the classical approach to determining fault gouge friction of applying constant machine drive velocity as the imposed boundary condition (e.g. Marone, 1998), as shear stress control can lead to catastrophic failure in the event of progressively weakening slip. Controlled total shear displacements of 2–6 mm were achieved in this way. Data on the frictional strength and rate-dependence of friction are obtained and a full Rate and State Friction (RSF) description is derived. In an attempt to understand the likely mechanisms determining frictional behaviour, microstructures of the samples are analysed. Finally, we discuss the implications of our findings for understanding induced seismicity in the Carboniferous source rocks beneath the Groningen gas reservoir.

## 2. Experimental methods

### 2.1. Approach

As indicated above, to achieve our aim of quantifying the effects of possible coal content on fault strength and slip stability below the Groningen reservoir, we performed experiments to measure the frictional sliding strength and rate-dependence of the coefficient of friction of simulated shale-coal fault gouges at in-situ Groningen gas field conditions. The starting materials were analysed using X-ray diffraction (XRD) and organic petrology, proximate and ultimate analysis. Microstructural analysis was performed on deformed gouge samples, in an attempt to understand the observed frictional behaviour.

We use the rate and state friction (RSF) approach to quantify our experimental data. From an RSF point view, if fault rocks exhibit an increase in frictional strength upon increased sliding rate, i.e. velocity strengthening behaviour, they are not prone to generating accelerating slip and are termed conditionally stable (Scholz, 2019). On the other hand, when the frictional strength of a fault rock decreases upon increased sliding rate, the fault rock exhibits velocity weakening behaviour. This may result in repetitive slip instabilities, or stick-slip events, which are viewed as the laboratory equivalent of earthquakes (Brace and Byerlee, 1966; Marone, 1998; Scholz, 1998).

### 2.2. Starting materials, sample preparation and direct shear assembly

The samples used in all experiments were prepared from Upper Carboniferous shale/siltstone material, from the Groningen gas field, and from a Polish coal, of similar age, rank and origin to the Groningen gas field source rocks (De Jager and Visser, 2017; Nowak, 2004). The Carboniferous shale/siltstone samples were collected from core obtained from the SDM-1 well in the seismogenic centre of the Groningen field. This material consists of 55 wt% quartz, 10 wt% feldspar and 35 wt% phyllosilicates, determined by XRD analysis - for details see Hunfeld et al. (2017). The coal samples used were high volatile bituminous coal collected from Brzeszcze Mine (Seam 364), in the Upper Silesian Basin of Poland (Hol et al., 2011; Van Bergen et al., 2006). It has a vitrinite reflectance of 0.77 ± 0.05% and has a vitrinite content of 60.1 wt%, alongside liptinite 9.8 wt%, inertinite 30.1 wt%, and total organic carbon (TOC) 69.6 wt% (Gensterblum et al., 2010; Hol et al., 2011). The Brezeszcze coal contains 74.1 wt% carbon, 5.3 wt% hydrogen, 1.4 wt% nitrogen, 0.7 wt% sulphur, 18.5 wt% oxygen, as well as 2.9 wt% moisture and 5.2 wt% ash (mineral) content (Hol et al., 2011). XRD analyses performed at the Reactor Institute at Delft

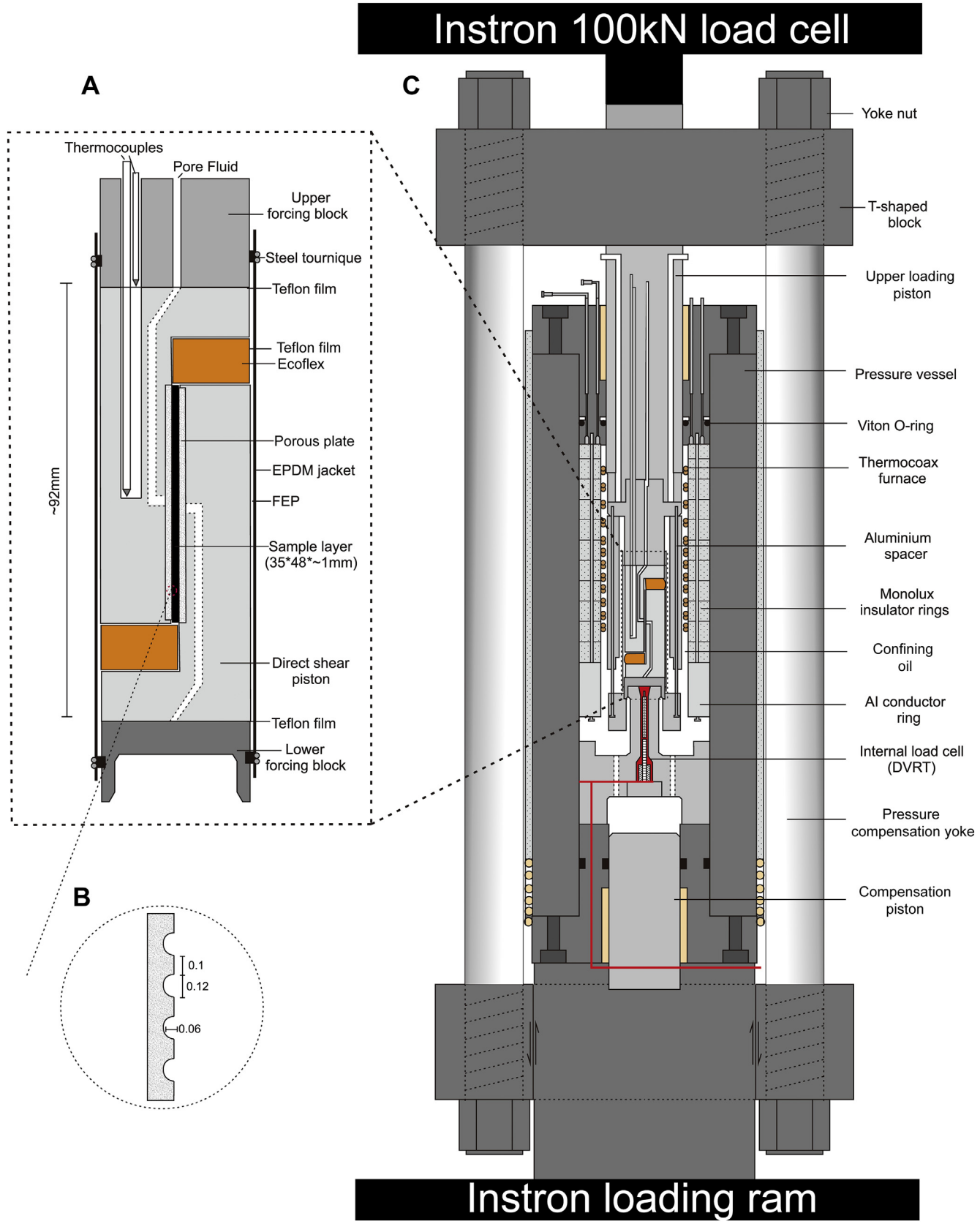


**Fig. 2.** Schematic cross-sections showing a) the present direct-shear sample assembly, (b) the groove pattern machined into in the porous stainless steel plates used to grip the sample layer, and c) the triaxial testing apparatus used to shorten the sample assembly, and hence shear the sample, under in-situ conditions. Modified after Verberne et al. (2014).

University of Technology show the minerals present to be quartz, dolomite, kaolinite and carbonate.

Simulated gouge samples were prepared by crushing and sieving fragments of Carboniferous shale/siltstone drillcore, and of a mined coal block, to obtain a grain size < 50 μm. The end member materials were mixed by mass to obtain solid volume fractions that were systematically varied in the range 0–100 vol% (see Table 1). Samples of these mixtures were tested using a cylindrical, direct shear assembly (diameter 35 mm and length ~ 70.1 mm), comprising two opposing, semi-cylindrical, L-shaped pistons (⌊), designed for direct shear testing in a triaxial deformation apparatus (following Samuelson and Spiers, 2012 – refer Fig. 2). Each L-shaped piston consists of a cylindrical, 35 mm diameter × 12 mm high base supporting a ~ 58 mm long semi-cylindrical "leg", housing a ~ 35 × 48 $mm^2$, grooved piston face in contact with the sample (Fig. 2a). The piston face consists of an embedded, sintered stainless-steel porous plate or frit, which ensured even distribution of the pore-fluid over the sample layer in wet experiments. The groove pattern, spark-eroded into the porous frit, comprised a set of 0.1 mm regularly spaced, semi-circular grooves 0.12 mm in diameter, i.e. cutting 0.06 mm into the frit (Fig. 2b).

Prior to each experiment, a gouge layer with an initial thickness of generally ~1 mm (see details in Table 1) was prepared by distributing ~1.5–2.9 g of powdered gouge mixture evenly over one of the direct shear piston faces. This was then pre-compacted at ~20 MPa for ~2 min using a bench press and a purpose-made support jig. The sample produced consisted of a briquette-like plate of simulated coal-shale fault gouge, measuring 35 mm in width by ~48 mm in length. The second L-shaped direct shear piston was subsequently placed face down on the pressed sample to sandwich it within the shear assembly (see Fig. 2a). The shear assembly was then jacketed, along the length of the sample using a thin, heat-shrinking, fluorinated ethylene propylene (FEP) sleeve to provide support, and the displacement-accommodating voids characterizing the shear assembly were filled with soft, Ecoflex polymer plugs (Fig. 2a), held in place using Teflon tape. The Ecoflex is easily extruded upon shortening the sample assembly, offering negligible resistance to piston motion and hence to shearing of the sample without contaminating the sample. Circular Teflon sheets were placed onto the base of the direct shear pistons to reduce shear resistance between the pistons and the load-transmitting forcing blocks. The entire assembly, i.e. the L-shaped forcing blocks or pistons, the sample layer and the displacement-accommodating Ecoflex plugs were then jacketed in an EPDM rubber sleeve of ~1.4 mm thickness, which was finally sealed against the cylindrical base of the pistons using wire torniques (see Fig. 2a). Note that pilot runs not presented here showed that the pre-compaction stress and the initial thickness of the samples has little effect on the results obtained during shearing, provided that the pre-compaction stress does not exceed the effective normal stress employed in the shearing stage.

### 2.3. Testing machine and experimental procedure

A total of 21 direct shear experiments were performed using a conventional triaxial testing machine, referred to as the Shuttle Machine (see Verberne et al., 2014), equipped with the internal direct shear assembly described above. The Shuttle Machine comprises a yoke-compensated, constant-volume, internally heated, oil-medium pressure vessel, located within an electrically actuated, servo-controlled Instron loading frame. A schematic cross-section of the pressure vessel is given in Fig. 2c (modified after Verberne et al., 2014).

The Instron was operated in ram-position control mode in all experiments, employing linear ramp functions to achieve fixed ram displacement rates or else position-hold mode to maintain fixed ram position. The PID settings of the position controller were set, taking into account the damping effect of friction at the loading piston seals within the pressure vessel (O-rings, Fig. 2c), such that imposed displacement-time ramps were faithfully followed by the Instron system without oscillation. This was verified in numerous trial runs.

When performing individual experiments, compressive ram displacement is transmitted to the direct shear assembly and sample via an internal titanium load cell, fixed in the base of the upwardly advancing pressure vessel, which is bolted to the Instron ram. Axial reaction, hence sample loading, is provided via a stationary upper loading piston supported by the Instron frame and external, 100 kN Instron load cell. The internal load cell allows measurement of axial force, independently of seal friction on the upper piston (Fig. 2c), with an accuracy equivalent to a sample shear stress of ~0.02 MPa.

The confining medium used in the present experiments was silicone-oil. Confining pressure was generated using a compressed-air-driven diaphragm pump, and controlled at the desired set-point using an ISCO 65D volumetric (syringe) pump (c.f. Hol and Spiers, 2012), operated in constant pressure mode with a control accuracy of ± 0.05 MPa. Pore fluid gains access to the sample through an internal bore in the upper loading piston (Fig. 2c). In the present experiments, its pressure was controlled using a second ISCO 65D pump. Sample heating in the Shuttle Machine is achieved using an internal Thermocoax furnace element, using a three-term CAL2300 industrial controller to regulate oil temperature near the sample to within 0.1 °C of the set-point test temperature. Sample temperature is measured using a thermocouple located in a bore in the upper direct shear piston within a few mm of the sample layer (Fig. 2a).

In the present paper, all experiments employed a sample temperature of 100 °C and a Terzaghi effective confining pressure, hence a Terzaghi effective normal stress ($\sigma_n^{eff}$) acting on the simulated fault gouge layer, of 40 MPa (refer Fig. 2a). According to lithological density logs and downhole measurements made by the field operator (NAM, 2013, 2016, see also Van Eijs, 2015), the total in-situ vertical stress within the Groningen reservoir is presently ~65 MPa, the horizontal stress is ~40 MPa, the pore fluid pressure is 8–15 MPa, the temperature is ~100 °C, and fault dips seen in seismic sections are ~70 degrees, implying effective normal stresses approaching 40 MPa on faults at the reservoir base. The chosen experimental conditions are therefore closely consistent with the in-situ temperature and effective normal stresses expected on faults in the Carboniferous shale/siltstone substrate directly below the reservoir at a burial depth of ~3000 m. Pore fluids used included distilled (DI) water, $CH_4$, Argon and laboratory air, with some tests being performed under vacuum. In each experiment, the sample assembly, initially drained to the lab air, was first heated to 100 °C at a confining pressure of ~20 MPa and left to equilibrate for ~15 h (overnight). Following evacuation, the pore fluid was then introduced into the sample and pressurized to 15 MPa at a confining pressure of ~20 MPa. The confining pressure was subsequently increased to 55 MPa and left the system for ~3 h to equilibrate before shearing. The pore fluid type and pressure employed in each experiment are summarized in Table 1. We conducted so called velocity-stepping (VS), constant velocity (CS), slide-hold-slide (SHS), and slide-unload-slide (SUS) experiments (see Table 1). For readers not familiar with friction testing methods, a schematic illustration of the displacement-time (hence velocity-time) path associated with each type of experimental sequence is shown in Fig. 3. In the VS experiments, samples were sheared at a constant velocity (V) of 1 μm/s for ~2.5 mm shear displacement, after which the loading rate was instantaneously stepped in the range 0.1–100 μm/s over total displacements up to almost 6 mm (generally in the sequence 1–0.1-1-10-100-10-1-0.1 μm/s). In the CS experiments, samples were sheared at a single fixed velocity (V) between 0.1 and 100 μm/s to displacements of ~2.5–3.5 mm. We also performed one SHS experiment (Sample SHS_1, 50:50 vol% coal-shale), in which the sample was sheared at a constant velocity (V) of 1 μm/s interrupted by hold intervals in the range 10–400,000 s. Recall that the hold intervals were achieved by operating the Instron in piston-hold control mode. We further report two SUS experiments (SUS_1 and SUS_2 - both 50:50 vol% coal-shale), following a sequence of slide-unload-reslide, employing a loading and unloading rate of 1 μm/s. Note

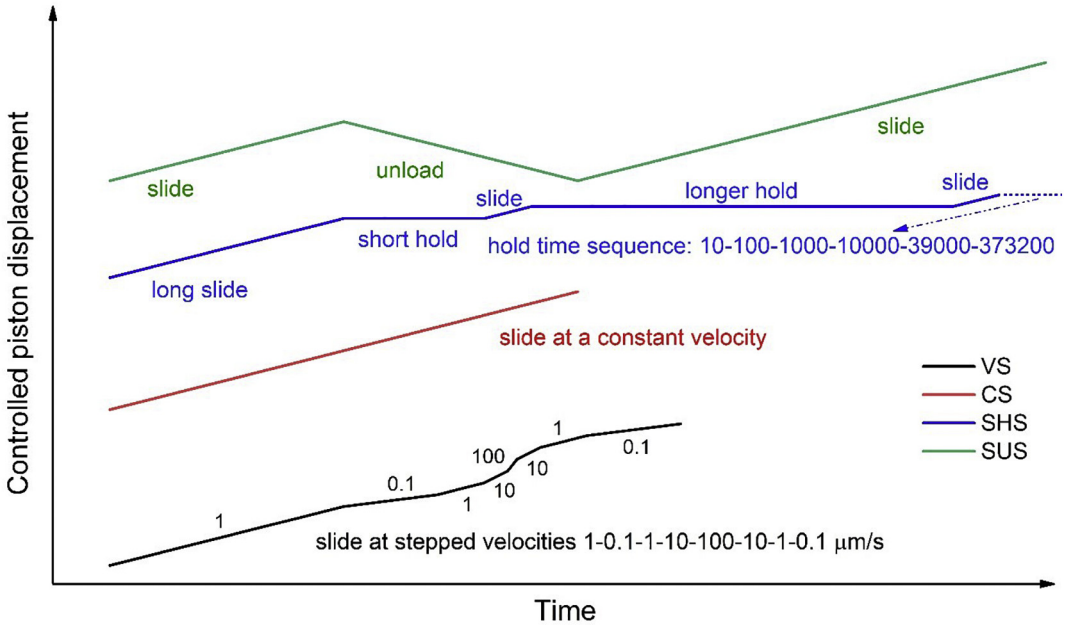


**Fig. 3.** Schematic illustration of displacement-time (hence velocity-time) paths imposed via the Instron loading ram in the present velocity stepping (VS), constant velocity (CS), slide-hold-slide (SHS), and slide-unload-slide (SUS) experiments. Final unloading is not shown.

that the effective normal stress on the simulated gouges was maintained at 40 MPa in all stages of all experiments.

### 2.4. Post-test sample treatment

After each experiment, the direct shear setup was dismantled, and intact fragments of the sheared gouge layers were recovered and oven-dried for several days. XRD analysis was performed on fragments extracted from the body of the gouge and from clear principal slip zones. Fragments for microstructural analysis were impregnated using Araldite 2020 epoxy resin. Following curing, sections of the impregnated fragments were cut and polished in an orientation parallel to the shear direction and perpendicular to the shear plane. The microstructure of the fragments was investigated using a Leica optical microscope and a Table-Top SEM. To ensure sufficient conduction to allow SEM analyses with minimal sample charging, the sample was first coated with a 5–8 nm thin layer of platinum. The samples investigated were imaged in backscattered electron (BSE) mode, using an acceleration voltage of 5–15 kV.

### 2.5. Data acquisition, processing and analysis

Internal axial force (hence shear force acting on the sample surface – see Fig. 2), confining pressure, pore fluid pressure, sample temperature and loading piston displacement were measured in each experiment and the signals logged at a rate of 20 Hz using a 16-bit National Instruments AD converter and logging system (for details, see Hunfeld et al., 2017, plus original data description given by Liu et al., 2019). During long hold intervals in the experiment SHS_1, the signal logging rate was switched to 0.2 Hz. The data were processed to yield sample shear stress versus shear displacement data corrected for machine stiffness (see details and processed data in Liu et al., 2019). The frictional strength of the samples was characterised by defining the apparent coefficient of sliding friction ($\mu$) as the ratio of sample shear stress ($\tau$), i.e. the measured internal axial force per unit sample surface, over the effective normal stress ($\sigma_n^{eff}$), assuming zero cohesion, that is as

$$\mu = \tau / \sigma_n^{eff} \quad (1)$$

where $\sigma_n^{eff} = \sigma_n - P_f$. Here $\sigma_n$ represents the normal stress or confining pressure employed in the experiments, and $P_f$ represents the pore fluid pressure.

The rate-dependence of friction was quantified using the Rate and State dependent Friction (RSF) theory (Dieterich, 1978, 1979; Ruina, 1983), coupled with the empirical Dieterich-type "aging law" (e.g. Marone, 1998):

$$\mu = \mu_0 + a \ln\left(\frac{V}{V_0}\right) + b \ln\left(\frac{V_0 \theta}{D_c}\right) \quad (2)$$

with

$$\frac{d\theta}{dt} = 1 - \frac{V\theta}{D_c} \quad (3)$$

Eq. (2) describes the evolution of friction coefficient $\mu$ from a reference steady state value ($\mu_0$) towards a new steady state value, over a critical slip distance ($D_c$), in response to an instantaneous change in sliding velocity from an initial sliding velocity ($V_0$) to a new sliding velocity ($V$). The state variable $\theta$, which describes the evolution of gouge friction via Eq. (3), is commonly viewed as the average lifespan of a population of grain-to-grain contacts (Marone, 1998). At steady state, i.e. when $d\theta/dt = 0$, Eq. (2) reduces to:

$$(a - b) = \frac{\mu - \mu_0}{\ln\left(V/V_0\right)} \quad (4)$$

where the parameter *(a–b)* reflects the rate-sensitivity of frictional coefficient. A positive (*a–b*) value indicates velocity strengthening behaviour, while a negative (*a–b*) value indicates velocity weakening behaviour, which is potentially unstable (Marone, 1998; Scholz, 1998). Here, we solve Eq. (2) simultaneously with an equation describing the elastic interaction with the testing machine via the stiffness, using Eq. (1) as a constraint. The values for $a$, $b$ and $D_c$ can then be obtained as the solutions of a nonlinear inverse problem using an iterative least-squares minimization method (Blanpied et al., 1995; Ikari et al., 2009), thereby obtaining a full RSF description of the material from our experiments. In performing RSF inversion, departures from steady state frictional sliding were corrected for by means of linear detrending of hardening or softening behaviour (see Fig. 4c). A detailed description is given by Blanpied et al. (1995).

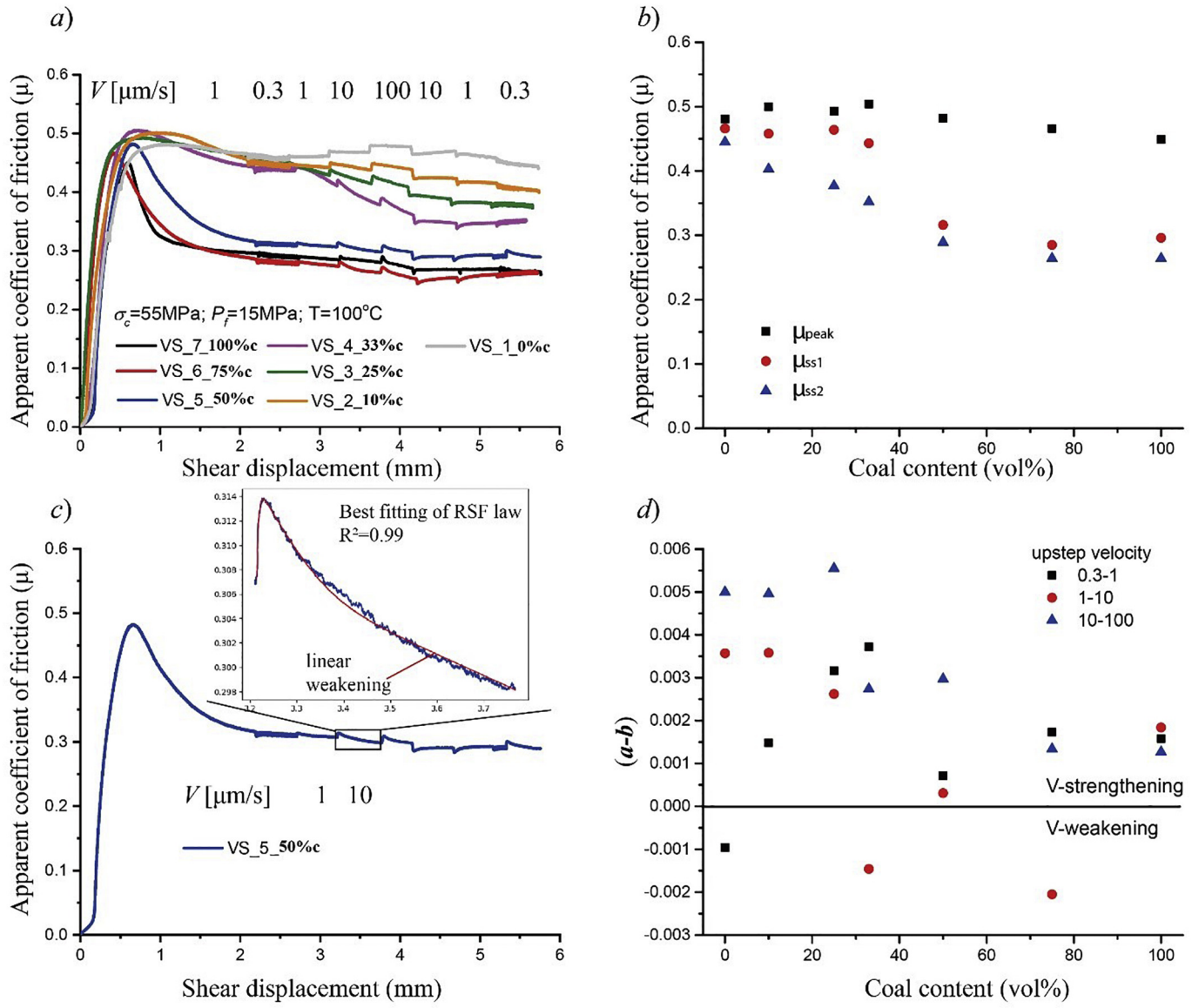


**Fig. 4.** Effect of coal content (vol%) on frictional behaviour of samples tested with DI water at 15 MPa pore pressure. a) Apparent coefficient of friction (μ) against shear displacement. b) Apparent coefficient of friction (μ) against coal content (vol%). c) Results of experiment VS_5, illustrating best fitting of a full RSF law to the experimental data obtained at velocity step from 1 to 10 μm/s. d) (a–b) values, obtained from upward velocity steps using a full RSF fit, versus coal content. The downstep data were similar but showed more scatter.

## 3. Results

### 3.1. Mechanical data

Key data obtained from the 21 experiments performed are listed in Table 1. All frictional strength data are summarized, including $\mu_{peak}$, $\mu_{ss1}$, and $\mu_{ss2}$. Here, $\mu_{peak}$ represents the peak frictional coefficient obtained at 0.42–1.26 mm shear displacement, $\mu_{ss1}$ represents the (near) steady-state frictional coefficient obtained at ~2.2 mm shear displacement (before implementing any velocity steps in sliding velocity), and $\mu_{ss2}$ represents the steady-state frictional coefficient obtained at ~5.7 mm shear displacement (near the end of the experiments). The individual RSF parameters *a*, *b* and $D_c$, and the rate-sensitivity parameter *(a–b)*, obtained for upward stepping data in all velocity-stepping experiments are summarized in Table 2, as it is these that are most relevant to rupture nucleation (Marone, 1998). Representative mechanical data are plotted in Figs. 4–8, and the typical microstructure of the samples after shearing is shown in Figs. 9 and 10.

#### 3.1.1. Effects of coal content on μ and (a–b) in tests at 15 MPa pore water pressure

Typical apparent frictional coefficient ($\mu$) versus displacement curves obtained in velocity stepping experiments (Exp. VS_1-VS_7), on samples containing 0–100 vol% coal and tested with DI water at 15 MPa pore pressure, are shown in Fig. 4. Those samples with a coal content less than 50 vol%, show near-linear initial loading up to a peak friction coefficient approaching 0.5, followed by minor slip weakening reaching quasi steady-state friction values $\mu_{ss1}$ at ~2.2 mm shear displacement (before velocity stepping) of ~0.45, independently of the presence or content of coal. Increased slip weakening is seen at larger (velocity stepping) displacements especially in samples with moderate coal content (Fig. 4a, b). By contrast, samples that contain 50 vol% coal or more (Exp. VS_5, VS_6 and VS_7) show sharp, post-peak slip weakening from peak friction values ($\mu_{peak}$) of ~0.45 to a steady state value ~0.3 - see Fig. 4b. These samples behaved more or less identically to pure coal (Exp. VS_7). The steady-state frictional coefficient of samples consisting of 50 vol% coal or more is accordingly lower than samples with < 50 vol% coal by ~0.15 (Fig. 4b).

**Table 2**
Summary of RSF data obtained in the upward velocity-steps employed in all velocity stepping experiments reported in this paper.

| Exp./Sam. | $V_0$ [μm/s] | $V$ [μm/s] | $a$–$b$ [−] | $a$ [−] | $b$ [−] | $D_c$ [mm] |
|---|---|---|---|---|---|---|
| VS_1 | | | | | | |
| V-step1 | 0.3 | 1 | −0.00096 | 0.00215 | 0.00311 | 0.07513 |
| V-step2 | 1 | 10 | 0.00357 | 0.00511 | 0.00154 | 0.00534 |
| V-step3 | 10 | 100 | 0.005 | 0.02305 | 0.01805 | 0.00195 |
| VS_2 | | | | | | |
| V-step1 | 0.3 | 1 | 0.00148 | 0.00247 | 0.00099 | 0.01878 |
| V-step2 | 1 | 10 | 0.00358 | 0.00608 | 0.00251 | 0.1097 |
| V-step3 | 10 | 100 | 0.00496 | 0.01316 | 0.0082 | 0.0125 |
| VS_3 | | | | | | |
| V-step1 | 0.3 | 1 | 0.00316 | 0.005 | 0.00184 | 0.03084 |
| V-step2 | 1 | 10 | 0.00262 | 0.00756 | 0.00493 | 0.04505 |
| V-step3 | 10 | 100 | 0.00555 | 0.01528 | 0.00972 | 0.0048 |
| VS_4 | | | | | | |
| V-step1 | 0.3 | 1 | 0.00372 | 0.00479 | 0.00107 | 0.01625 |
| V-step2 | 1 | 10 | −0.00146 | 0.00477 | 0.00623 | 0.00623 |
| V-step3 | 10 | 100 | 0.00274 | 0.00677 | 0.00403 | 0.00403 |
| VS_5 | | | | | | |
| V-step1 | 0.3 | 1 | 0.00072 | 0.00302 | 0.0023 | 0.06483 |
| V-step2 | 1 | 10 | 0.00031 | 0.00325 | 0.00295 | 0.05334 |
| V-step3 | 10 | 100 | 0.00297 | 0.07157 | 0.0686 | 0.02636 |
| VS_6 | | | | | | |
| V-step1 | 0.3 | 1 | 0.00173 | 0.00265 | 0.00092 | 0.13604 |
| V-step2 | 1 | 10 | −0.00205 | 0.00323 | 0.00528 | 0.07323 |
| V-step3 | 10 | 100 | 0.00134 | 0.00497 | 0.00364 | 0.03289 |
| VS_7 | | | | | | |
| V-step1 | 0.3 | 1 | 0.00158 | 0.0017 | 0.00012 | 0.07985 |
| V-step2 | 1 | 10 | 0.00184 | 0.00336 | 0.00151 | 0.0705 |
| V-step3 | 10 | 100 | 0.00127 | 0.00925 | 0.00799 | 0.01952 |
| VS_8 | | | | | | |
| V-step1 | 0.1 | 1 | −0.00459 | 0.00367 | 0.00826 | 0.064 |
| V-step2 | 1 | 10 | −0.00227 | 0.00092 | 0.00318 | 0.13558 |
| V-step3 | 10 | 100 | −0.00039 | 0.00191 | 0.00229 | 0.13566 |
| VS_9 | | | | | | |
| V-step1 | 0.1 | 1 | −0.01 | stick-slip | | |
| V-step2 | 1 | 10 | −0.00395 | 0.00275 | 0.00671 | |
| V-step3 | 10 | 100 | 0.00137 | 0.00142 | 0.00005 | |
| VS_10 | | | | | | |
| V-step1 | 0.1 | 1 | −0.0007 | stick-slip | | |
| V-step2 | 1 | 10 | −0.00426 | 0.00246 | 0.00672 | 0.02065 |
| V-step3 | 10 | 100 | 0.0009 | 0.00129 | 0.00039 | 0.06594 |
| VS_11 | | | | | | |
| V-step1 | 0.1 | 1 | −0.00068 | 0.00275 | 0.00343 | 0.00318 |
| V-step2 | 1 | 10 | 0.01575 | 0.00368 | −0.01207 | 0.00382 |
| V-step3 | 10 | 100 | 0.00197 | 0.02953 | 0.02756 | 0.0004 |
| VS_12 | | | | | | |
| V-step1 | 0.1 | 1 | −0.0122 | stick-slip | | |
| V-step2 | 1 | 10 | −0.00102 | 0.00323 | 0.00425 | 0.02943 |
| V-step3 | 10 | 100 | −0.00012 | 0.01328 | 0.0134 | 0.01578 |
| VS_13 | | | | | | |
| V-step1 | 0.1 | 1 | −0.00234 | stick-slip | | |
| V-step2 | 1 | 10 | −0.00122 | 0.00162 | 0.00284 | 0.11611 |
| V-step3 | 10 | 100 | 0.00048 | 0.0358 | 0.03532 | 0.04444 |
| VS_14 | | | | | | |
| V-step1 | 0.1 | 1 | −0.0005 | stick-slip | | |
| V-step2 | 1 | 10 | −0.0008 | 0.003 | 0.0038 | 0.053 |
| V-step3 | 10 | 100 | 0.0021 | 0.0031 | 0.001 | 0.05 |

Attention is restricted to the upward steps, as it is these that are most relevant to rupture nucleation (Marone, 1998).

The ($a$–$b$) data obtained from the velocity stepping experiments VS_1-VS_7 represented in Fig. 4a, using a full RSF approach, are plotted in Fig. 4d as a function of coal content. We plot upward stepping data only, as again it is these that are most relevant to rupture nucleation (Marone, 1998). These data show that almost all ($a$–$b$) values are in the range of +0.001 to +0.006, with the magnitude decreasing with increasing coal content. A relatively sudden drop in *(a–b)* is evident at coal contents beyond 50 vol% (see Fig. 4d), paralleling the change in frictional strength seen in Fig. 4a, b. Overall, though, at a pore water pressure of 15 MPa and a confining pressure of 55 MPa, experiments VS_1-VS_7 show stable, velocity-strengthening behaviour, regardless of coal content and velocity steps employed.

### *3.1.2. Effects of varying pore fluids on μ and (a–b) in tests on 50:50 samples*

The frictional behaviour of 50:50 (vol%) shale-coal mixtures (Exp. VS_5, VS_8–10, and VS_13–14) subjected to velocity stepping in the presence of water, $CH_4$ and Argon at a pore fluid pressure of 15 MPa is illustrated in Fig. 5, along with data from tests performed under vacuum, room dry and (1 atm) water-saturated conditions. The 50:50 (vol %) composition was assumed representative for samples with ≥50 vol % coal (based on Fig. 4). All runs (all pore fluid conditions) show the marked slip weakening behaviour seen in samples with 50 vol% or more coal tested with water at 15 MPa (cf Figs. 4a and 5a). From Fig. 5a and b, it is clear that varying pore fluid composition or state has little effect on friction, though the presence of water may reduce friction slightly compared to vacuum and gas-saturated conditions. However, a significant influence of pore fluids and pore pressure on the velocity dependence of friction can be seen in Fig. 5c. Whereas the 50:50 (vol%) composition sample exposed to water at a pore fluid pressure of 15 MPa showed stable, velocity-strengthening behaviour, samples exposed to $CH_4$, Ar, vacuum, air and even to water at 1 atm showed velocity-weakening or near neutral behaviour, at velocities stepped in the range 0.1–10 μm/s. Stick-slip events were observed in Exp. VS_8-VS_10 and VS_13–14 (exposed to vacuum, air, water at 1 atm, $CH_4$ and Ar, respectively) at low sliding velocities, i.e. at 0.1–1 μm/s (but not in samples exposed to water at a pore fluid pressure of 15 MPa proving that the observed stick-slips are not machine oscillations).

### *3.1.3. Effects of varying single sliding rate and loading path on friction*

The evolution of frictional coefficient with shear displacement in 50:50 (vol%) shale-coal samples (Exp. CS_1–4), measured at different, constant sliding velocities and at 15 MPa DI water pore pressure is shown in Fig. 6. The frictional coefficient systematically decreases with increasing sliding velocity, demonstrating velocity weakening behaviour as opposed to velocity strengthening seen under the same conditions, but at larger displacements, in V-stepping test VS_5 on 50:50 (vol%) material (Fig. 5a, c).

The slide-hold-slide (SHS) loading path data (experiment SHS_1, 50:50 vol% composition, 15 MPa DI water) shown in Fig. 7 indicates a clear yet minor strength recovery or healing effect ($\Delta\mu$), upon resliding, followed by slip-weakening to achieve a new quasi steady state. The magnitude of restrengthening ($\Delta\mu$) in experiment SHS_1 increases with the logarithm of hold time ($t$), and is well described by the equation $\Delta\mu = \beta \log\left(1 + \frac{t}{t_c}\right)$ (e.g. Dieterich, 1972; Im et al., 2017), where $\beta$ = 0.00173 and $t_c$ = 472.11 s (Fig. 7b).

The frictional behaviour exhibited by 50:50 (vol%) samples SUS_1–2 and CS_4 (15 MPa pore water pressure), which were more or less fully unloaded and then reloaded in the steady state sliding regime, is illustrated in Fig. 8. This shows that the marked slip-weakening behaviour seen in samples with coal volume fractions ≥50 vol% is limited to small initial displacements (2–3 mm) and did not occur after unloading, reloading and reshear. Note that the variability in peak and steady-state friction levels seen in these experiments (Fig. 8) may be caused by the different shearing velocities and sample thicknesses used (Table 1), in line with the effects of shearing rate illustrated in Fig. 6. Also note the clear increase in steady state friction of ~0.025 in the experiments sheared at 100 μm/s after the unload-slide step.

### *3.2. Microstructural and XRD observations*

The microstructure of sample VS_8 (50:50 vol% shale-coal mixture tested under vacuum) is shown in Fig. 9, and indicates a clear coal-rich boundary shear as well as coal-rich Y- and R- shear bands (using the terminology of Logan et al., 1992). Similar microstructures were observed in all samples with 50 vol% coal content that could be recovered,

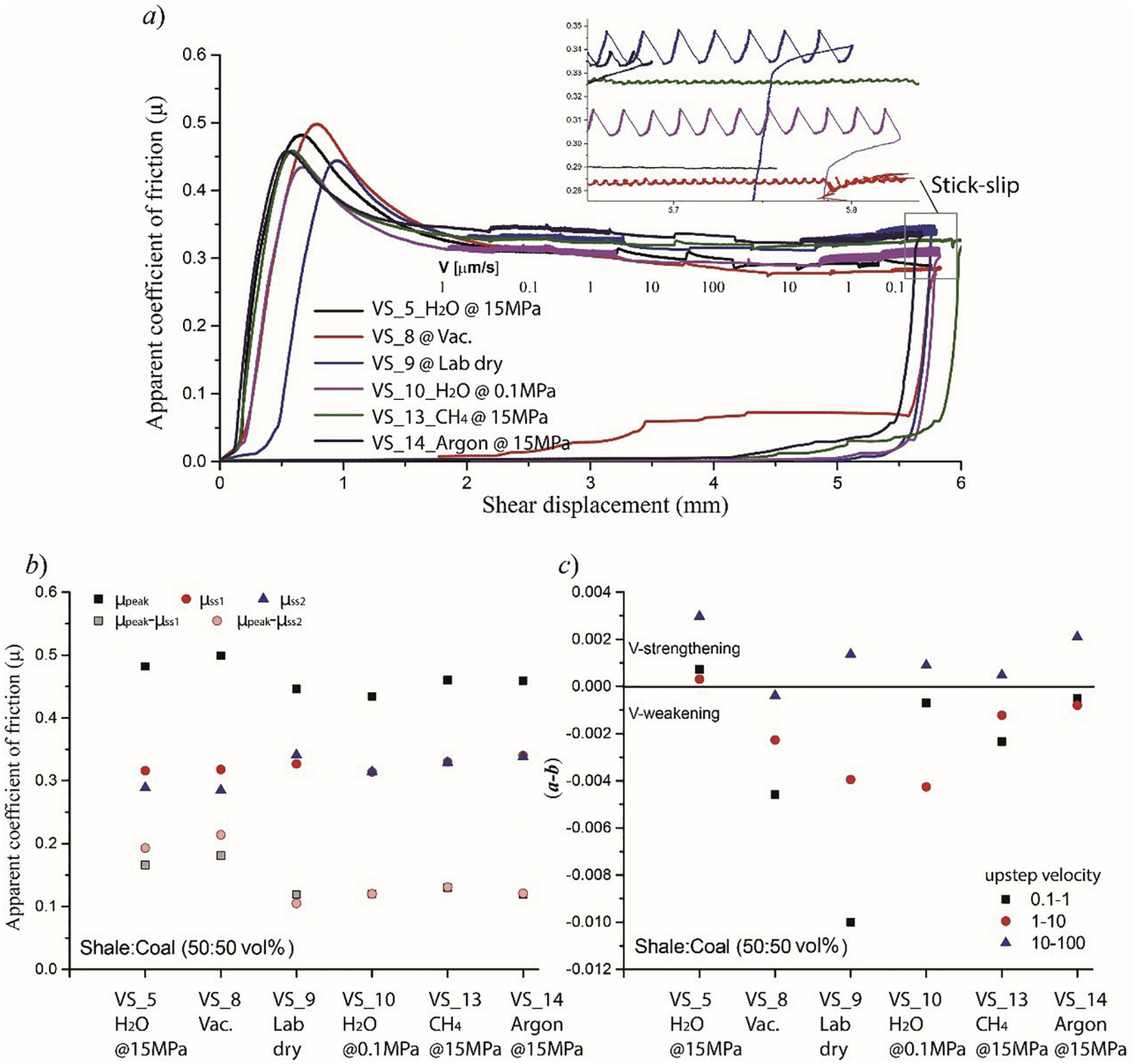


**Fig. 5.** Effects of varying pore fluid conditions on frictional behaviour of 50:50 (vol%) shale-coal samples sheared at an effective normal stress of 40 MPa and at 100 °C. a) Friction (μ) versus shear displacement for the pore fluids shown in Table 1. b) Correlation between frictional coefficient values (μ) and pore fluid composition and state. c) (a–b) obtained from upward velocity steps using a full RSF fit for the various pore fluids employed in this paper.

as opposed to the samples with < 50 vol% coal content where coal-rich shear bands were not clearly observed (see Fig. 10a vs. b). This may suggest strain localization in weak coal-rich shear bands. We note here that use of SEM for microstructural observations on coal-rich samples which were impregnated using carbon-bearing epoxy is potentially problematic, and that more discriminatory techniques for preparing coal samples need to be found in future. XRD analysis of the principal boundary slip surface and of the body of the pure coal gouge sample VS_7 (tested using DI water at 15 MPa) shown in Fig. 11 indicates no detectable difference in carbon structure between these sites.

## 4. Discussion

We have reported 21 direct shear experiments on coal-shale mixtures designed to simulate coal-bearing fault gouges developed in the Carboniferous source rock underlying the Slochteren sandstone reservoir in the Groningen gas field. The experiments were conducted under field-relevant conditions, as listed in Table 1. The results for samples tested in velocity stepping (VS) mode, using DI water at 15 MPa pore pressure, demonstrate that increasing coal content causes i) a decrease in initial peak friction, ii) an increase in subsequent slip weakening, becoming sharp at coal contents of 50 vol%, and iii) a decrease in velocity strengthening *(a–b)* values. Pore fluid type and pore fluid pressure mostly have little effect on frictional strength, at least in the case of 50:50 (vol%) coal-shale mixtures, but can strongly influence the rate-dependence of friction, with “dry” and gas saturated samples showing negative (a–b) values. Interestingly, in contrast to the VS data obtained using water at a pore pressure of 15 MPa, constant slip rate (CS) data obtained on 50:50 (vol%) samples at the same conditions show velocity weakening behaviour at all displacements. Other effects

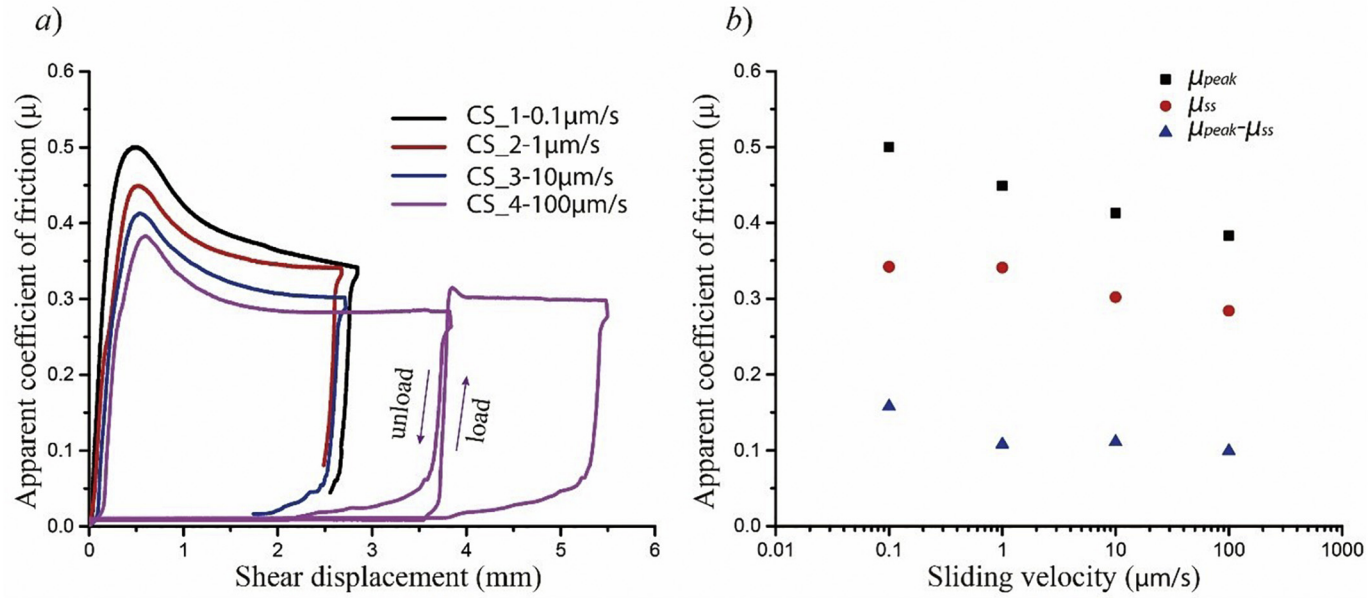


**Fig. 6.** a) Frictional coefficient (μ) vs. displacement data for 50:50 (vol%) shale-coal samples tested at different, constant sliding velocities in the presence of $H_2O$ pore fluid at 15 MPa pressure. b) Equivalent data showing friction (μ) measured at different displacements versus sliding velocity.

of shearing/loading history on 50:50 (vol%) samples at these conditions, include minor healing in both SHS tests (Dieterich healing) and SUS tests.

In the following, we first attempt to elucidate the mechanisms responsible for the marked slip-weakening behaviour seen at coal contents ≥50 vol%. We then discuss the velocity-dependence of friction and the effects of shearing/loading history and pore fluid type and pressure. Finally, we consider the implications of our findings for the frictional strength and induced seismic potential of faults in the Carboniferous substrate beneath the Groningen gas reservoir.

### 4.1. Mechanisms causing slip-weakening

#### 4.1.1. Role of coal content

Our experiments demonstrate that all samples with ≥50 vol% coal, including the 100 vol% Brzeszcze coal sample VS_7, showed marked slip weakening behaviour, from a peak friction coefficient approaching 0.5 to a (near) steady state value around only 0.3, regardless of the experimental conditions employed. By contrast, samples containing < 50 vol% coal showed only minor slip weakening. Recalling that the mineral content of the 100% coal sample material is < 5.2 wt%, which is not likely to have a significant influence, the implication is that the observed slip-weakening is directly related to the coal content. However, the mechanism causing slip- or shear-weakening of the coal

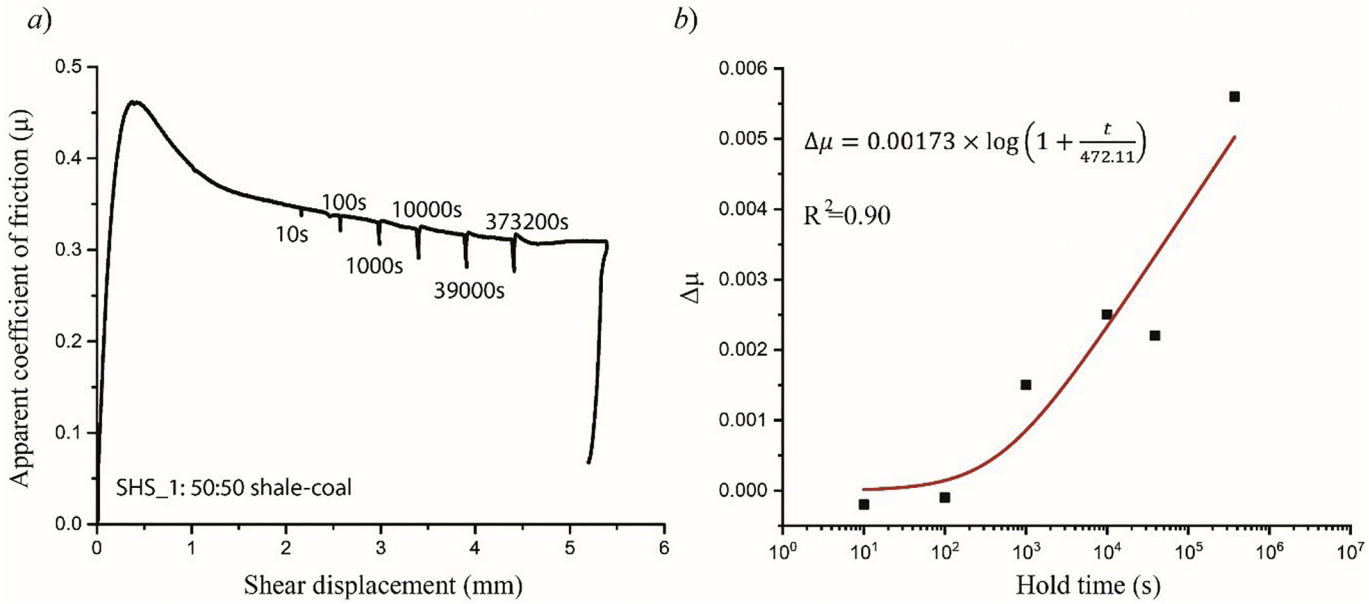


**Fig. 7.** Slide-hold-slide data for 50:50 (vol%) shale-coal sample SHS_1 tested with $H_2O$ at a pore fluid pressure of 15 MPa. a) Frictional coefficient versus shear displacement, showing slide-hold-slide testing sequence. b) Transient peak healing or post-hold frictional restrengthening plotted as a function of the logarithm of hold time. The black solid squares represent the experimental data derived from Fig. 7a, and the red line represents the best fit line healing trend. (For interpretation of the references to colour in this figure legend, the reader is referred to the web version of this article.)

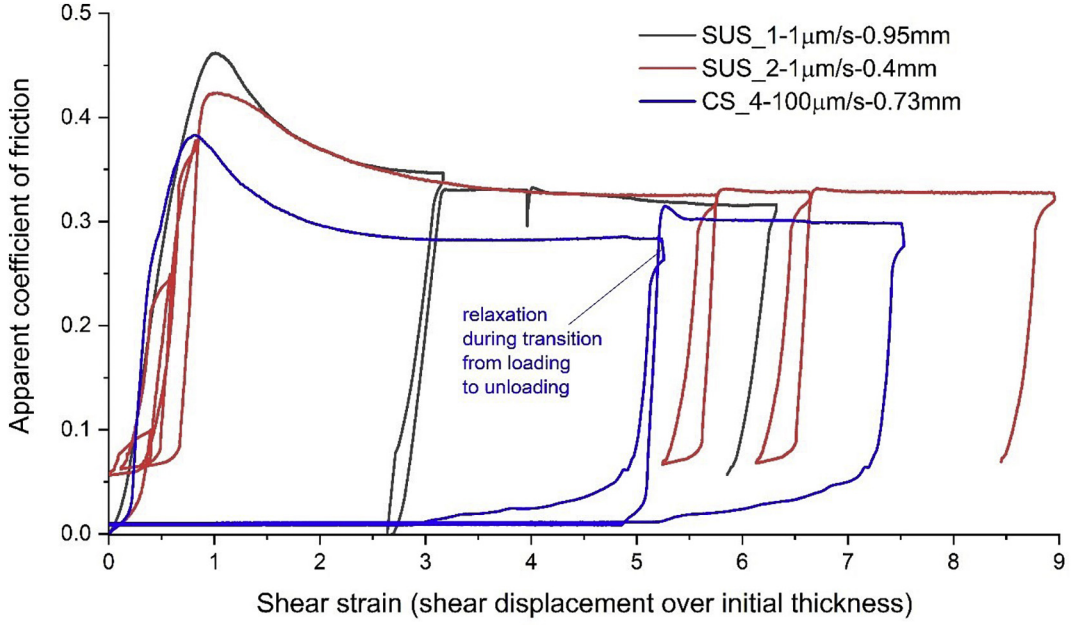


**Fig. 8.** Frictional coefficient (μ) versus shear strain for 50:50 (vol%) shale-coal samples exposed to $H_2O$ at a pore fluid pressure of 15 MPa and sheared in a variety of slide-unload-slide sequences employing different sliding velocities and different starting gouge layer thickness.

component remains an open question. In the following, we attempt to gain some insights from the literature.

We first consider whether graphitization could have occurred, as seen in high velocity friction experiments. Oohashi et al. (2011), for example, performed friction experiments on both amorphous carbon and graphite using a rotary shear apparatus under conditions of normal stress of 0.5–2.8 MPa and slip rates of 50 μm/s – 1.3 m/s (as opposed to our 0.1–100 μm/s) in atmospheres of air and nitrogen. Their experiments showed a) a steady-state friction coefficient of 0.54 for amorphous carbon at slow slip rates versus 0.1 for graphite at all slip rates, b) major slip-weakening of the amorphous phase, at slip rates > 10 mm/s, to a steady-state μ-value of 0.1, and c) XRD and TEM evidence of graphitization of the amorphous carbon during shear at high slip rates. The authors suggested that large shear strains, short-lived flash heating, and/or stress concentrations at asperity contact points may cause graphitization of amorphous carbon, even at low temperatures and pressures under anoxic environments. Similar friction experiments, performed by Kuo et al. (2014) on natural samples collected from the 2018 Wenchuan earthquake slip zone, also showed graphitization of carbonaceous minerals due to frictional heating at seismic slip rates. More importantly, molecular dynamics simulations of sliding at the interface between amorphous carbon and diamond films, at a rate of 10 m/s, performed by Ma et al. (2014), show that covalent bond reorientation, phase transformation and structural ordering preferentially occur in localized bands in amorphous carbon film, and that this shear localization causes weakening.

Returning to our experiments, the temperature and sliding rates employed mean that lubrication effects (Di Toro et al., 2011) due to sample-scale frictional heating and hence graphitization (e.g. Oohashi et al., 2013) can be eliminated. Nonetheless, the high volatile

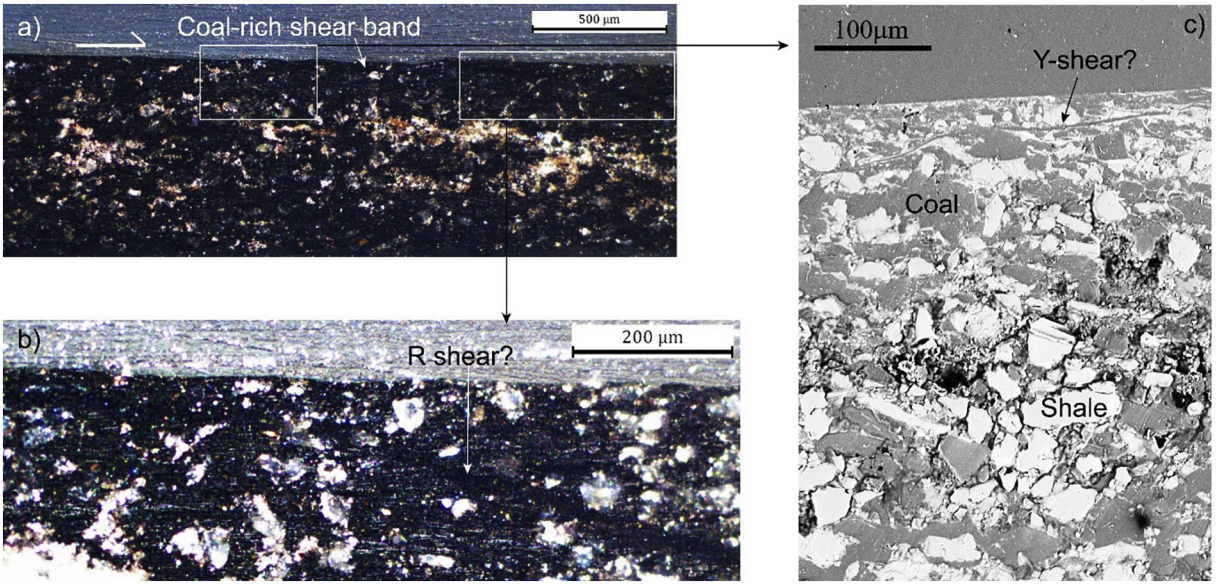


**Fig. 9.** Microstructure of 50:50 vol% shale-coal sample VS_8 after direct shear under vacuum dry conditions. a) and b) were imaged in reflected light, while c) was imaged in backscattered electron (BSE) mode using a Table Top SEM. Shear sense is right lateral.

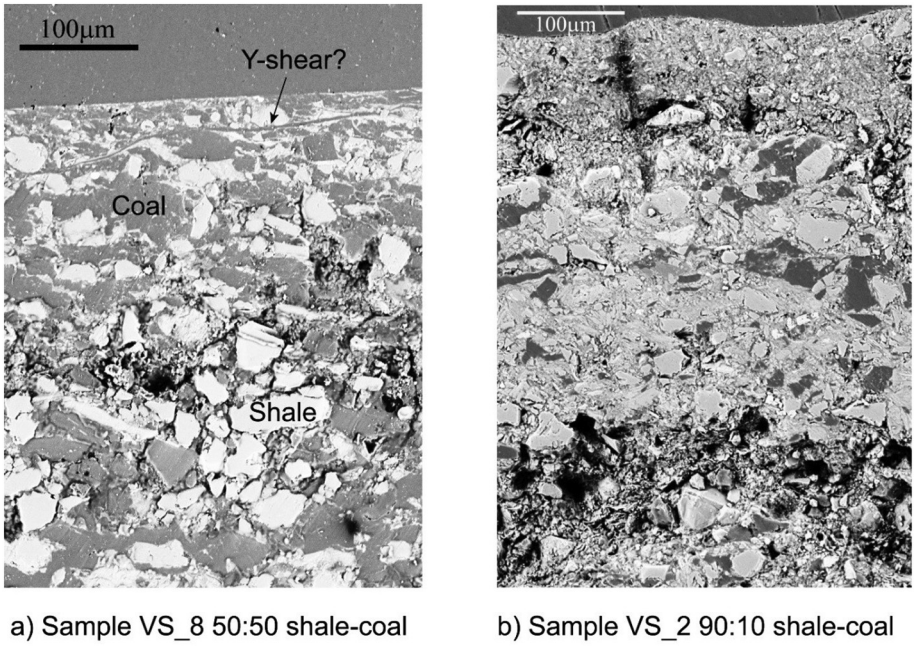


**Fig. 10.** SEM-BSE images of samples VS_8 (50:50 vol% shale-coal; vacuum dry) versus VS_2 (90:10 vol% shale-coal; tested using DI water as pore fluid at 15 MPa). Shear sense is right lateral.

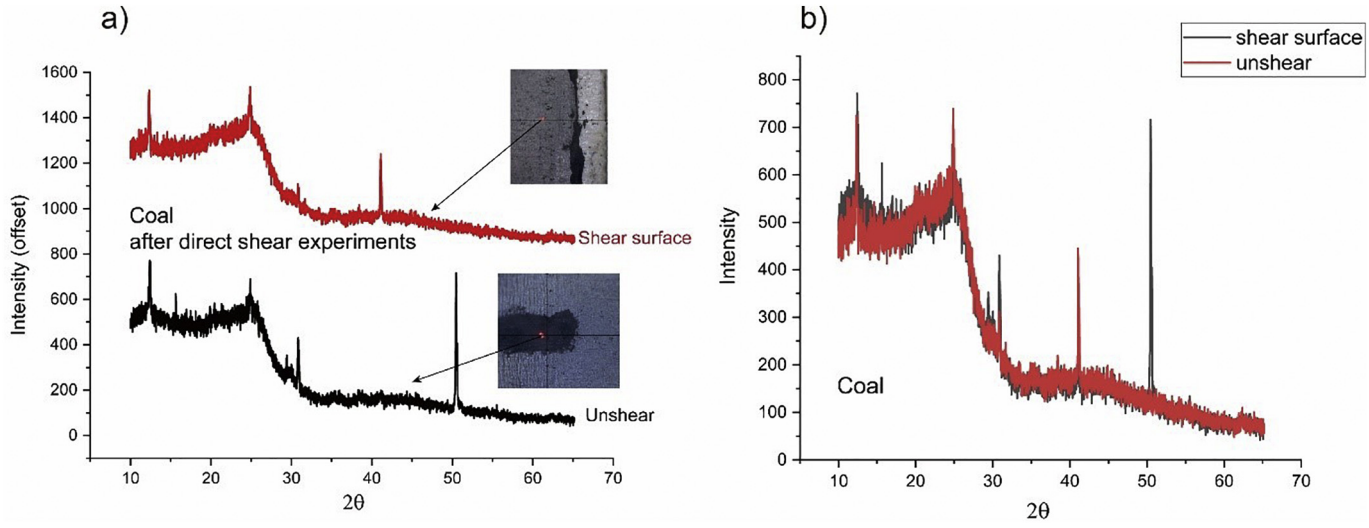


**Fig. 11.** a) XRD diffractogram for samples retrieved from the boundary sliding surface and gouge body of the 100% coal sample VS_7 tested with DI water as pore fluid at 15 MPa. b) Overlay comparison of the two XRD diffraction spectra shown in (a).

bituminous coal samples used in this study contain 74 wt% carbon. According to Takagi et al. (2004), such coals may exhibit a stacked or platy/layered structure, as suggested by our XRD analysis (see Fig. 11) and proposed in the model by Lu et al. (2001) based on XRD analysis of Australian coals ranging in rank from semi-anthracite to high volatile bituminous. In the Lu model, coal consists of both amorphous and crystalline (graphite-like) forms of carbon. These displayed frictional coefficients of respectively 0.54 and ~ 0.1 in the experiments of Oohashi et al. (2011), while the peak and steady state values seen in our coal-rich samples were ~ 0.5, and ~ 0.3. On this basis, it seems possible that slip weakening seen in our coal-rich and 100% coal samples may have been caused by some increase in crystallinity of the coal during shear deformation (Kaneki and Hirono, 2019), even at low slip rates. To test this hypothesis further, new research will be conducted in future using Raman spectroscopy and advanced XRD analysis (Kaneki and Hirono, 2019; Lu et al., 2001; Potgieter-Vermaak et al., 2011).

In addition to the above, our microstructural observations on the 50:50 (vol%) sample from which intact fragments could be recovered (Sample VS_8 tested under vacuum) indicate that slip weakening is associated with strain localization occurring in coal-rich R-, Y- and boundary (B) shear bands (refer Figs. 4a and 9). To some extent, this is similar to weakening behaviour widely observed in the simulated phyllosilicate-bearing fault rocks, such as analogue mixtures of halite and kaolinite (Bos et al., 2000; Bos and Spiers, 2001) or halite and muscovite (Niemeijer and Spiers, 2005), quartz-muscovite or talc mixtures (Niemeijer, 2018), and quartz-illite-montmorillonite (Tembe et al., 2010). These studies demonstrated that slip weakening could largely be attributed to the development of a connected foliation of weak phyllosilicate (a geometric effect). Taken together with our mechanical data, these observations suggest that slip weakening and shear band localization in the 50–100 vol% coal samples occurred due to smearing of shear-weakening coal into the developing shear bands. This

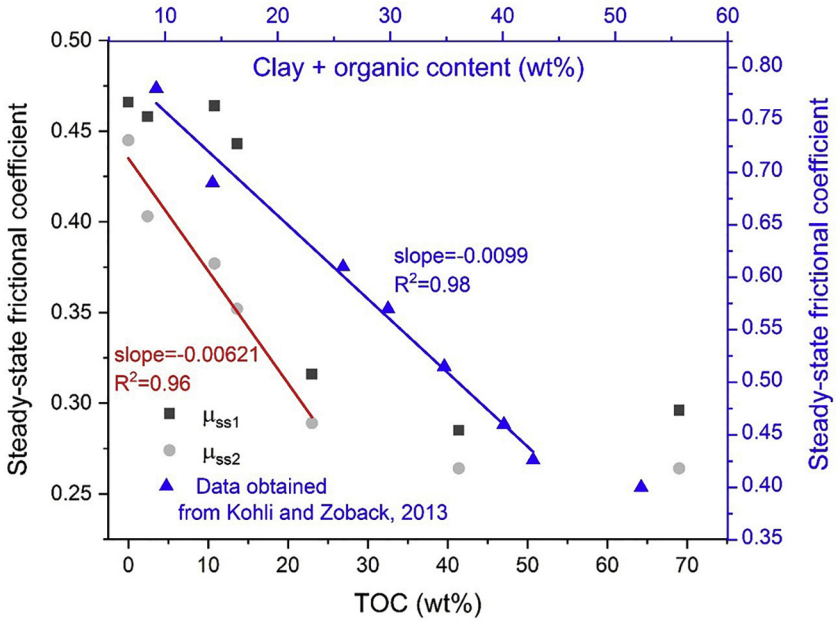


**Fig. 12.** Steady-state frictional coefficient obtained from our experiments and Kohli and Zoback (2013) as a function of total organic carbon (TOC, wt%). Note that the dots are the data points and the straight lines represent best fits to the present $\mu_{ss2}$ and Kohli-Zoback data only.

would also explain why slip weakening occurred during initial shearing but not during reshearing (see Fig. 8), with the shear weakening of "pure" coal being caused by the increase in crystallinity proposed above (rather than any effects of the 5.2 wt% mineral content of the coal starting material used in this study). A possible implication of the marked slip weakening seen in coal-rich samples at low shear strains is that the inferred localization on coal-rich shear bands might provide a mechanism for nucleating unstable (accelerating) slip, hence seismogenesis, on coal-rich fault segments with minor offset. However, whether this mechanism will operate at seismic slip velocities is as yet unknown.

#### 4.1.2. Role of total organic carbon (TOC) content

It follows from the above that the slip weakening effect caused by coal component of our samples should be related to total organic carbon content. To assess this further, we replotted the data from Fig. 4b as a function of wt% TOC, as shown in Fig. 12. Here, the wt% TOC content of samples VS_1-VS_7 was obtained using the fact that the 100% coal material contains 69.6 wt% TOC, and converting the volume fraction of coal in the shale-coal mixtures (0–100 vol% coal) into weight % (yielding 0–69.6 wt% TOC). With reference to Fig. 12, note from the $\mu_{ss2}$ data, obtained at large displacements, that the weakening effect already occurs with only ~2.4 wt% TOC (Sample VS_2 with 10 vol% or 3 wt% coal). The difference between $\mu_{ss1}$ and $\mu_{ss2}$ values further shows that this weakening requires significant displacement to be realised. The weakening with increasing TOC demonstrated by the $\mu_{ss2}$ data is roughly linear with increasing TOC up until ~23 wt%, with a slope of −0.006. At TOC contents from 23 wt% (coal content ≥50 vol %, i.e. coal content ≥33 wt%), the steady state frictional coefficient approaches that of the 100% coal material, suggesting that all deformation is accommodated within the coal bands, as inferred in Section 4.1.1, and presumably within purely organic sub-bands. Similar findings were also reported by Kohli and Zoback (2013) who performed friction experiments on shale samples collected from three hydrocarbon reservoirs. Their experiments showed that frictional strength of the shale samples systemically decreased from ~0.8 to ~0.42 with increasing clay and organic contents at a near-linear rate of 0.0099 (see Fig. 12). Note, however, that total organic content of the shale samples used by Kohli and Zoback lay in the range 1.86–5.70 wt% which is much lower than the simulated samples used in our study. This presumably explains the larger absolute values of steady-state frictional coefficient reported by Kohli and Zoback, compared to the values reported by us at TOC values above 5 wt%.

### 4.2. Velocity dependence of friction

#### 4.2.1. Effects of loading path and pore fluid

The *(a–b)* values obtained from our velocity stepping (VS) experiments shown in Fig. 4d show that velocity strengthening behaviour predominates for samples exposed to water at a pore fluid pressure of 15 MPa, regardless of coal content. This is not consistent with our observations from constant velocity (CS) experiments under the same PT conditions (Fig. 6) which showed that the friction coefficient for 50:50 (vol%) samples systematically deceased with increasing sliding velocity, implying velocity weakening.

We will first address whether this inconsistency might be caused by poor reproducibility in the constant velocity experiments due to sample variability. To do so, we consider the mean values and associated standard deviations for $\mu_{peak}$ and $\mu_{ss}$ in 50:50 (vol%) experiments CS_2, VS_5, SHS_1, SUS_1 and SUS_2 at a velocity step of 1 μm/s. The mean friction coefficients for peak and quasi steady-state are 0.455 and 0.335, while the standard deviations are 0.021 and 0.014, respectively. With reference to Fig. 6, this variability might explain the apparent velocity weakening seen in experiments CS_1 and CS_2, performed at 0.1 and 1 μm/s, respectively, but is not large enough to explain the velocity weakening behaviour observed in samples CS_2 - CS_4, i.e. at velocities of 1–100 μm/s.

A possible explanation for the thus-confirmed velocity weakening behaviour observed in the constant velocity 50:50 (vol%) experiments at velocities ≥1 μm/s might be that the pore fluid becomes locally overpressurized at high sliding velocities. Faulkner et al. (2018), see Figure 11 in their paper, reported numerical solutions demonstrating a clear weakening effect of increasing sliding velocity (0.05–10 μm/s) on apparent gouge friction curves, caused by development of excess pore fluid pressure due to shear-driven compaction of the gouge layer with increasing displacement. In the early stages of our faster (10–100 μm/s), 50:50 (vol%) experiments at constant velocity, shear-enhanced compaction might easily occur faster than pore fluid drainage, thus leading to an increase of pore fluid water pressure and producing an apparent velocity weakening not seen in velocity stepping tests (which

were sheared at 1 μm/s to around 2 mm displacement and then stepped under potentially better drained conditions). Unfortunately, we do not have sufficiently accurate pore fluid volume change or gouge compaction data to verify this hypothesis. However, an additional argument for the development of local fluid overpressures in the experiments that were sheared at high constant velocity (> 1 μm/s) can be found in the results of the unloading-loading cycle in experiment CS_4, sheared at 100 μm/s. During the re-sliding, the apparent frictional coefficient is higher than the previous steady state value (Figs. 6 and 8), which is consistent with the dissipation of (some) fluid overpressure during the unloading-reloading phase and the corresponding recovery in effective normal stress. In fact, friction has recovered to a value higher than the steady state value in the experiment sheared at 10 μm/s, indicating velocity strengthening similar to what was obtained in the velocity stepping experiments. On this basis, we infer that the apparent velocity weakening behaviour observed in our constant velocity experiments for 50:50 (vol%) coal-shale samples (see Fig. 6) was indeed most likely caused by overpressure effects.

#### 4.2.2. Effects of pore fluid on rate dependence of friction

We now consider the effects of pore fluid type and pressure on rate-dependent friction, using the RSF. *(a–b)* values obtained from our velocity stepping data, notably the up-steps, which are most directly relevant to the increasing velocities associated with the nucleation stage of an earthquake rupture (Marone, 1998). Fig. 5c summarises the effects of different pore fluid types and pressures on the rate-dependent friction behaviour (i.e. *(a–b)* values) seen in our 50:50 (vol%) shale-coal samples. The 50:50 (vol%) samples tested with DI water as pore fluid at 15 MPa, and indeed all coal compositions tested at 15 MPa pore water pressure, show positive and consistently higher *(a–b)* values than those obtained for 50:50 (vol%) compositions using other pore fluid conditions.

In an attempt to explain this apparently special effect of water at high pressure, we plot the *(a–b)* values shown in Table 2 versus sliding velocity for the 50:50 (vol%) samples indicating the various pore conditions employed – see Fig. 13. Careful inspection of Fig. 13 shows a tendency for a transition from velocity weakening to velocity strengthening at a slip rate of ~10 μm/s under lab dry conditions, in samples exposed to water at atmospheric pressure, and in samples exposed to pure gases ($CH_4$ and Ar) at 15 MPa. This suggests that some common factor controls the rate-dependence of friction in these specific experiments (VS_9, VS_10, VS_13, VS_14). Surprisingly, the 50:50 (vol %) sample tested under vacuum dry conditions (VS_8) exhibited velocity weakening at all slip rates, whereas all gouge compositions showed predominant velocity strengthening when exposed to water at 15 MPa. The implication is that the presence of water in itself is not a determining factor but that water at a high pore fluid pressure may play an important role in promoting velocity strengthening in our coal rich samples.

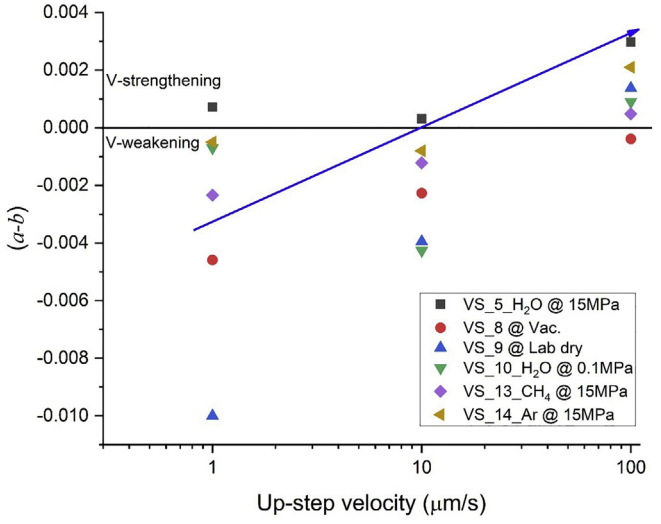


**Fig. 13.** (a–b) values obtained for the 50:50 (vol%) shale-coal samples plotted against sliding velocity, with the various pore fluid conditions imposed indicated.

We have no firm explanation for this unusual behaviour at present. More research is needed for a better understanding, such as experiments employing a broader range of slip rates, or investigation of the effects of higher compressibility of pore water added at 1 atm pressure due to incomplete pore saturation. We note, also, that unlike mineral gouges, coal exhibits marked stress-strain-sorption behaviour when exposed to water or/and $CH_4$ (Liu et al., 2018; Liu et al., 2016). This behaviour leads to swelling/shrinkage strains that strongly depend on chemical activity (pressure) of the adsorbing fluid as well as on the Terzaghi effective stress supported by the solid grain framework. Such effects could conceivably result in competition between compaction and dilatation during shearing of coal gouge, leading to a complex rate-dependence of friction similar to that produced by competition between dilatant granular flow and compaction by pressure solution seen in mineral gouges (Chen and Spiers, 2016; Niemeijer and Spiers, 2007).

### 4.3. Implications for fault strength and stability in the Groningen Carboniferous

Our experiments show that the presence of coal in volume fractions ≥ 50 vol% (TOC content ≥ 23 wt%) can cause marked slip-weakening of simulated Carboniferous shales/siltstone fault gouges derived from the Groningen field, followed by (near) steady-state sliding (Fig. 4). The rather sharp slip weakening behaviour superficially suggests increased potential for unstable, i.e. accelerating fault slip and earthquake nucleation in coal-rich fault segments, given appropriately low stiffness of the surrounding rock volume. However, the reloading data shown in Fig. 8, and the microstructure shown in Fig. 9, suggest that significant slip-weakening occurs only in previously unsheared material in which coal rich shear bands have yet to develop (Logan et al., 1992; Marone, 1998). In our experiments, strain localization and slip weakening may have been caused by changes in the molecular structure of coal within the developing shear bands. However, regardless of the mechanisms, our findings suggest that slip-weakening is unlikely to occur on coal-rich faults in the Groningen Carboniferous, at the low slip velocities associated with rupture nucleation, as previous tectonic displacements will invariably have exceeded the 1–2 mm slip weakening distance observed in our experiments. In addition, the SHS experiment on 50:50 (vol%) composition material illustrated in Fig. 7 demonstrates only very minor healing (restrengthening) effects, with transient peak healing in friction increasing with the logarithm of hold time (s) at a linearized rate of only 0.00117. Post-healing slip weakening effects are correspondingly minor. Compared with healing rates typically measured in quartz or carbonate gouges (Chen et al., 2015; Nakatani and Scholz, 2004), representative for other Groningen units, we accordingly expect little or no effect of healing on frictional strength of faults in coal-bearing Carboniferous sections, even after geological periods of healing, which again points to very limited scope for slip weakening and seismogenic rupture nucleation in the case of fault reactivation.

Aside from the slip weakening effect, our experiments do indicate that the presence of coal, especially in amounts ≥ 50 vol%, can locally reduce the frictional strength of faults that displace the Groningen Carboniferous shale/siltstone sequence, from ~0.45 to ~0.3. In natural faults, smearing of gouges derived from different formations cut by the fault results in a degree of mixing that increases with the displacement on the fault relative to the thickness of the displaced formations (c.f. Shale Gouge Ratio, see Yielding et al., 1997). However, as coal seams are expected to be relatively rare (widely spaced) and thin in the Carboniferous shales and siltstone underlying the Groningen gas reservoir,

weak, fault gouge patches with coal contents > 50 vol%, will be both rare and very limited in slip-parallel extent. Since the present coal-rich samples also show steady state, largely velocity strengthening, non-healing behaviour after shearing beyond 1–2 mm at in-situ, water-saturated conditions, neither coal-coal nor smeared-out coal-rich fault patches are expected to be prone to seismic slip nucleation. By contrast, under dry and gas-saturated ($CH_4$, Argon) conditions, our 50:50 (vol%) shale-coal samples exhibited velocity-weakening behaviour, and even stick-slip, at sliding velocities of 0.1–1 and 1–10 μm/s (i.e. $(a–b) < 0$, in Fig. 5c). However, since the Carboniferous in Groningen is expected to be fully water (brine) saturated, our results imply that faults cutting coal seams in the Groningen Carboniferous will generally exhibit stable, aseismic slip if (re)activated. At the same time, possible destabilizing effects of the mechanical heterogeneity caused by weak coal-coal and coal-smear patches cannot be completely eliminated (Buijze et al., 2017; Kaneki and Hirono, 2019; Kohli and Zoback, 2013; Tembe et al., 2010). Similarly, the slip and velocity dependence of friction in coal-bearing fault segments, at velocities associated with seismic slip initiated elsewhere on a given fault, remain unknown.

## 5. Conclusions

This paper has investigated the effects of coal content (0–100 vol%) on the frictional properties of faults in the Carboniferous shale/siltstone source rocks underlying the seismogenic Groningen gas reservoir. This was done by performing direct shear experiments on simulated fault gouges, prepared from crushed shale/siltstone plus coal mixtures, under near in-situ reference conditions of temperature (100 °C), in-situ stress and pore fluid pressure (15 MPa), using a variety of pore fluids ranging from water to methane and argon. The Carboniferous shale/siltstone material was collected from Groningen gas field drillcore. The coal used was bituminous coal mined from the Upper Silesian Basin sequence in Poland, which is of similar age and broad origin to the Groningen source rocks. The experiments were performed at low sliding velocities (0.1–100 μm/s) simulating slip-patch nucleation rates. A full Rate and State Friction (RSF) analysis was employed to describe the friction data produced. The main conclusions are as follows:

1. Simulated Carboniferous shale/siltstone gouge with zero coal content shows a steady-state friction coefficient (μ) of ~0.47 under water-saturated reference conditions. Adding coal to the gouge has little effect on frictional strength until the coal content reaches 50 vol% in volume. At and beyond this point (i.e. at 50–100 vol% coal content), the gouges show marked slip-weakening behaviour over a few mm of displacement, from a peak friction coefficient approaching 0.5 towards a steady state value of ~0.3, regardless of the experimental conditions employed.
2. Limited microstructural observations suggest that the observed slip-weakening behaviour reflects localization caused by simultaneous smearing plus strain weakening of the coal component to form weak, through-going coal-rich shear bands, of R-, Y- and boundary types. Previous work on coal and carbon structure suggest that this strain weakening within coal-rich shear bands may involve a change in coal molecular structure towards a crystalline graphite-like form. This behaviour offers a possible mechanism for nucleating unstable slip. However, unloading-reloading experiments show that slip weakening, and hence any potential for unstable slip, is limited to small initial displacements (~2 mm), and does not occur during slip reactivation at larger displacements.
3. A single slide-hold-slide experiment performed at 15 MPa pore water pressure indicates that the frictional strength of 50:50 (vol%) shale/siltstone-coal mixtures increases transiently, or “heals”, during hold periods, followed by slip-weakening to re-establish steady state upon reshearing. The transient peak healing (re-strengthening) effect increases with the logarithm of hold time at a linearized rate of 0.00173, demonstrating only a very minor effect of healing (and subsequent slip weakening) on frictional strength.
4. Velocity stepping experiments demonstrate stable, velocity strengthening behaviour of the shale-coal samples at in-situ stress, pore water pressure and temperature conditions, regardless of coal content. By contrast, under vacuum/room dry and gas-saturated ($CH_4$ and Argon) conditions, and when saturated with water at 1 atm, 50:50 (vol%) shale-coal mixtures exhibit unstable, velocity-weakening, and even stick-slip behaviour.
5. On the basis of the above findings (1–4), we conclude that gouge-filled faults in the Carboniferous shale/siltstone formation underlying the Groningen gas reservoir are likely to exhibit stable, non-accelerating slip behaviour at rupture nucleation velocities at in-situ conditions, even when coal-bearing, though the mechanisms controlling frictional behaviour remain unclear. Effects of macroscopic compositional heterogeneity on fault stability, specifically weak patches caused by coal faulting and coal smearing, cannot be eliminated, though all evidence presented here suggests that these patches will be small, rare and resistant to the nucleation of seismogenic slip.

## Declaration of competing interest

The authors declare that they have no known competing financial interests or personal relationships that could have appeared to influence the work reported in this paper.

## Acknowledgement

This research was funded by the Nederlandse Aardolie Maatschappij B.V. (NAM), the operator of the Groningen gas field. First author Liu was supported in the latter stages of the work by the National Natural Science Foundation of China (NSFC project No. 41802230). A.R. Niemeijer was funded through ERC Starting Grant SEISMIC (335915) and by the Netherlands Organization for Scientific Research (NWO) through VIDI grant 854.12.011. Dr. Jianye Chen is thanked for discussions and HPT Lab technicians, Gert Kastelein and Floris van Oort, are thanked for their superb technical support. Last but not least, the anonymous reviewers are highly appreciated for their valuable comments and suggestions to improve this paper.

## Author statement

All descriptions are accurate and also agreed by all authors.

## References

Blanpied, M.L., Lockner, D.A., Byerlee, J.D., 1995. Frictional slip of granite at hydrothermal conditions. J. Geophys. Res. Solid Earth 100, 13045–13064. https://doi.org/10.1029/95JB00862.

Bos, B., Spiers, C.J., 2001. Experimental investigation into the microstructural and mechanical evolution of phyllosilicate-bearing fault rock under conditions favouring pressure solution. J. Struct. Geol. 23, 1187–1202. https://doi.org/10.1016/S0191-8141(00)00184-X.

Bos, B., Peach, C.J., Spiers, C.J., 2000. Frictional-viscous flow of simulated fault gouge caused by the combined effects of phyllosilicates and pressure solution. Tectonophysics 327, 173–194. https://doi.org/10.1016/S0040-1951(00)00168-2.

Brace, W., Byerlee, J., 1966. Stick-slip as a mechanism for earthquakes. Science 153, 990–992. https://doi.org/10.1126/science.153.3739.990.

Buijze, L., van den Bogert, P.A., Wassing, B.B., Orlic, B., ten Veen, J., 2017. Fault reactivation mechanisms and dynamic rupture modelling of depletion-induced seismic events in a Rotliegend gas reservoir. Neth. J. Geosci. 96, s131–s148. https://doi.org/10.1017/njg.2017.27.

Buijze, L., van den Bogert, P.A.J., Wassing, B.B.T., Orlic, B., 2019. Nucleation and arrest of dynamicrupture induced by reservoir depletion. J. Geophys. Res. SolidEarth 124, 3620–3645. https://doi.org/10.1029/2018JB016941.

Chen, J., Spiers, C.J., 2016. Rate and state frictional and healing behavior of carbonate fault gouge explained using microphysical model. J. Geophys. Res. Solid Earth 121, 8642–8665. https://doi.org/10.1002/2016JB013470.

Chen, J., Verberne, B.A., Spiers, C.J., 2015. Effects of healing on the seismogenic potential of carbonate fault rocks: experiments on samples from the Longmenshan Fault, Sichuan, China. J. Geophys. Res. Solid Earth 120, 5479–5506. https://doi.org/10.

1002/2015JB012051.
Cook, N.G.W., 1976. Seismicity associated with mining. Eng. Geol. 10, 99–122. https://doi.org/10.1016/0013-7952(76)90015-6.
De Jager, J., Visser, C., 2017. Geology of the Groningen field–an overview. Neth. J. Geosci. 96, s3–s15. https://doi.org/10.1017/njg.2017.22.
Di Toro, G., Han, R., Hirose, T., De Paola, N., Nielsen, S., Mizoguchi, K., Ferri, F., Cocco, M., Shimamoto, T., 2011. Fault lubrication during earthquakes. Nature 471, 494–498. https://doi.org/10.1038/nature09838.
Dieterich, J.I.I., 1972. Time-dependent friction in rocks. J. Geophys. Res. 77, 3690–3697. https://doi.org/10.1029/jb077i020p03690.
Dieterich, J.H., 1978. Time-dependent friction and the mechanics of stick-slip. In: Rock Friction and Earthquake Prediction. Springer, pp. 790–806. https://doi.org/10.1007/bf00876539.
Dieterich, J.H., 1979. Modeling of rock friction: 1. Experimental results and constitutive equations. J. Geophys. Res. Solid Earth 84, 2161–2168. https://doi.org/10.1029/JB084iB05p02161.
Ellsworth, W.L., 2013. Injection-induced earthquakes. Science 341, 1225942. https://doi.org/10.1126/science.1225942.
Elsworth, D., Spiers, C.J., Niemeijer, A.R., 2016. Understanding induced seismicity. Science 354, 1380–1381. https://doi.org/10.1126/science.aal2584.
Faulkner, D.R., Sanchez-Roa, C., Boulton, C., den Hartog, S., 2018. Pore fluid pressure development in compacting fault gouge in theory, experiments, and nature. J. Geophys. Res. Solid Earth 123, 226–241. https://doi.org/10.1002/2017JB015130.
Gensterblum, Y., Van Hemert, P., Billemont, P., Battistutta, E., Busch, A., Krooss, B., De Weireld, G., Wolf, K.-H., 2010. European inter-laboratory comparison of high pressure $CO_2$ sorption isotherms II: natural coals. Int. J. Coal Geol. 84, 115–124. https://doi.org/10.1016/j.coal.2010.08.013.
Guglielmi, Y., Cappa, F., Avouac, J.-P., Henry, P., Elsworth, D., 2015. Seismicity triggered by fluid injection–induced aseismic slip. Science 348, 1224–1226. https://doi.org/10.1126/science.aab0476.
Hol, S., Spiers, C.J., 2012. Competition between adsorption-induced swelling and elastic compression of coal at CO2 pressures up to 100 MPa. J. Mech. Phys. Solids 60, 1862–1882. https://doi.org/10.1016/j.jmps.2012.06.012.
Hol, S., Peach, C.J., Spiers, C.J., 2011. Applied stress reduces the $CO_2$ sorption capacity of coal. Int. J. Coal Geol. 85, 128–142. https://doi.org/10.1016/j.coal.2010.10.010.
Hunfeld, L., Niemeijer, A., Spiers, C., 2017. Frictional properties of simulated fault gouges from the seismogenic Groningen gas field under in situ P–T-chemical conditions. J. Geophys. Res. Solid Earth 122, 8969–8989. https://doi.org/10.1002/2017JB014876.
Ikari, M.J., Saffer, D.M., Marone, C., 2009. Frictional and hydrologic properties of a major splay fault system, Nankai subduction zone. Geophys. Res. Lett. 36, L20313. https://doi.org/10.1029/2009GL040009.
Im, K., Elsworth, D., Marone, C., Leeman, J., 2017. The impact of frictional healing on stick-slip recurrence interval and stress drop: implications for earthquake scaling. J. Geophys. Res. Solid Earth 122, 10102–10117. https://doi.org/10.1002/2017JB014476.
Kaneki, S., Hirono, T., 2019. Diagenetic and shear-induced transitions of frictional strength of carbon-bearing faults and their implications for earthquake rupture dynamics in subduction zones. Sci. Rep. 9, 7884. https://doi.org/10.1038/s41598-019-44307-y.
Kohli, A.H., Zoback, M.D., 2013. Frictional properties of shale reservoir rocks. J. Geophys. Res. Solid Earth 118, 5109–5125. https://doi.org/10.1002/jgrb.50346.
Kuo, L.-W., Li, H., Smith, S.A., Di Toro, G., Suppe, J., Song, S.-R., Nielsen, S., Sheu, H.-S., Si, J., 2014. Gouge graphitization and dynamic fault weakening during the 2008 Mw 7.9 Wenchuan earthquake. Geology 42, 47–50. https://doi.org/10.1130/G34862.1.
Liu, J., Spiers, C.J., Peach, C.J., Vidal-Gilbert, S., 2016. Effect of lithostatic stress on methane sorption by coal: Theory vs. experiment and implications for predicting in-situ coalbed methane content. Int. J. Coal Geol. 167, 48–64. https://doi.org/10.1016/j.coal.2016.07.012.
Liu, J., Fokker, P.A., Peach, C.J., Spiers, C.J., 2018. Applied stress reduces swelling of coal induced by adsorption of water. Geomech. Energy Environ. 16, 45–63. https://doi.org/10.1016/j.gete.2018.05.002.
Liu, J., Hunfeld, L.B., Niemeijer, A.R., Spiers, C.J., 2019. Frictional properties of simulated shale-coal fault gouges: implications for induced seismicity in source rocks below Europe's largest gas field. EPOS Reposit. v1. 10.24416/UU01-KQZUPZ.
Logan, J., Dengo, C., Higgs, N., Wang, Z., 1992. Fabrics of experimental fault zones: their development and relationship to mechanical behavior. In: International Geophysics. Elsevier, pp. 33–67. https://doi.org/10.1016/S0074-6142(08)62814-4.
Lu, L., Sahajwalla, V., Kong, C., Harris, D., 2001. Quantitative X-ray diffraction analysis and its application to various coals. Carbon 39, 1821–1833. https://doi.org/10.1016/S0008-6223(00)00318-3.
Ma, T.-B., Wang, L.-F., Hu, Y.-Z., Li, X., Wang, H., 2014. A shear localization mechanism for lubricity of amorphous carbon materials. Sci. Rep. 4https://doi.org/10.1038/srep03662. 3662.
Majer, E.L., Baria, R., Stark, M., Oates, S., Bommer, J., Smith, B., Asanuma, H., 2007. Induced seismicity associated with enhanced geothermal systems. Geothermics 36, 185–222. https://doi.org/10.1016/j.geothermics.2007.03.003.
Marone, C., 1998. Laboratory-derived friction laws and their application to seismic faulting. Annu. Rev. Earth Planet. Sci. 26, 643–696. https://doi.org/10.1146/annurev.earth.26.1.643.
Nakatani, M., Scholz, C.H., 2004. Frictional healing of quartz gouge under hydrothermal conditions: 1. Experimental evidence for solution transfer healing mechanism. J. Geophys. Res. Solid Earth 109https://doi.org/10.1029/2001JB001522. B07201.
Nederlandse Aardolie Maatschappij B. V. (NAM), 2013. A Technical Addendum to the Winningsplan Groningen 2013 Subsidence, Induced Earthquakes and Seismic Hazard Analysis in the Groningen Field. NAM, Assen.
Nederlandse Aardolie Maatschappij B. V. (NAM), 2016. Technical Addendum to the Winningsplan Groningen 2016. NAM, Assen.
Niemeijer, A.R., 2018. Velocity-dependent slip weakening by the combined operation of pressure solution and foliation development. Sci. Rep. 8, 4724. https://doi.org/10.1038/s41598-018-22889-3.
Niemeijer, A.R., Spiers, C.J., 2005. Influence of phyllosilicates on fault strength in the Brittle–Ductile transition: insights from rock analogue experiments. Geol. Soc. Lond. Spec. Publ. 245, 303–327. https://doi.org/10.1144/GSL.SP.2005.245.01.15.
Niemeijer, A., Spiers, C., 2007. A microphysical model for strong velocity weakening in phyllosilicate-bearing fault gouges. J. Geophys. Res. Solid Earth. https://doi.org/10.1029/2007JB005008. 112.
Nowak, G.J., 2004. Facies studies of bituminous coals in Poland. Int. J. Coal Geol. 58, 61–66. https://doi.org/10.1016/j.coal.2003.08.006.
Oohashi, K., Hirose, T., Shimamoto, T., 2011. Shear-induced graphitization of carbonaceous materials during seismic fault motion: experiments and possible implications for fault mechanics. J. Struct. Geol. 33, 1122–1134. https://doi.org/10.1016/j.jsg.2011.01.007.
Oohashi, K., Hirose, T., Shimamoto, T., 2013. Graphite as a lubricating agent in fault zones: an insight from low-to high-velocity friction experiments on a mixed graphite-quartz gouge. J. Geophys. Res. Solid Earth 118, 2067–2084. https://doi.org/10.1002/jgrb.50175.
Potgieter-Vermaak, S., Maledi, N., Wagner, N., Van Heerden, J., Van Grieken, R., Potgieter, J., 2011. Raman spectroscopy for the analysis of coal: a review. J. Raman Spectrosc. 42, 123–129. https://doi.org/10.1002/jrs.2636.
Ruina, A., 1983. Slip instability and state variable friction laws. J. Geophys. Res. Solid Earth 88, 10359–10370. https://doi.org/10.1029/JB088iB12p10359.
Samuelson, J., Spiers, C.J., 2012. Fault friction and slip stability not affected by $CO_2$ storage: evidence from short-term laboratory experiments on North Sea reservoir sandstones and caprocks. Int. J. Greenh. Gas Control 11, S78–S90. https://doi.org/10.1016/j.ijggc.2012.09.018.
Scholz, C.H., 1998. Earthquakes and friction laws. Nature 391, 37–42. https://doi.org/10.1038/34097.
Scholz, C.H., 2019. The Mechanics of Earthquakes and Faulting. Cambridge University Presshttps://doi.org/10.1017/9781316681473.
Spetzler, J., Dost, B., 2017. Hypocentre estimation of induced earthquakes in Groningen. Geophys. J. Int. 209, 453–465. https://doi.org/10.1093/gji/ggx020.
Spiers, C.J., Hangx, S.J., Niemeijer, A.R., 2017. New approaches in experimental research on rock and fault behaviour in the Groningen gas field. Neth. J. Geosci. 96, s55–s69. https://doi.org/10.1017/njg.2017.32.
Takagi, H., Maruyama, K., Yoshizawa, N., Yamada, Y., Sato, Y., 2004. XRD analysis of carbon stacking structure in coal during heat treatment. Fuel 83, 2427–2433. https://doi.org/10.1016/j.fuel.2004.06.019.
Tembe, S., Lockner, D.A., Wong, T.F., 2010. Effect of clay content and mineralogy on frictional sliding behavior of simulated gouges: binary and ternary mixtures of quartz, illite, and montmorillonite. J. Geophys. Res. 115, B03416. https://doi.org/10.1029/2009JB006383.
Van Bergen, F., Pagnier, H., Krzystolik, P., 2006. Field experiment of enhanced coalbed methane-CO2 in the upper Silesian basin of Poland. Environ. Geosci. 13, 201–224. https://doi.org/10.1306/eg.02130605018.
Van Eijs, R.M.H.E., 2015. Neotectonic stresses in the Permian Slochteren Formation of the Groningen Field. In: KNMI Scientific Report, Report No. EP201510210531. NAM, Assen.
Van Eijs, R., Mulders, F., Nepveu, M., Kenter, C., Scheffers, B., 2006. Correlation between hydrocarbon reservoir properties and induced seismicity in the Netherlands. Eng. Geol. 84, 99–111. https://doi.org/10.1016/j.enggeo.2006.01.002.
Van Thienen-Visser, K., Breunese, J., 2015. Induced seismicity of the Groningen gas field: history and recent developments. Lead. Edge 34, 664–671. https://doi.org/10.1190/tle34060664.1.
Van Wees, J., Buijze, L., Van Thienen-Visser, K., Nepveu, M., Wassing, B., Orlic, B., Fokker, P., 2014. Geomechanics response and induced seismicity during gas field depletion in the Netherlands. Geothermics 52, 206–219. https://doi.org/10.1016/j.geothermics.2014.05.004.
Verberne, B., Spiers, C., Niemeijer, A., De Bresser, J., De Winter, D., Plümper, O., 2014. Frictional properties and microstructure of calcite-rich fault gouges sheared at sub-seismic sliding velocities. Pure Appl. Geophys. 171, 2617–2640. https://doi.org/10.1007/s00024-013-0760-0.
Westbrook, G.K., Kusznir, N.J., Browitt, C.W.A., Holdsworth, B.K., 1980. Seismicity induced by coal mining in Stoke-on-Trent (U.K.). Eng. Geol. 16, 225–241. https://doi.org/10.1016/0013-7952(80)90017-4.
Yielding, G., Freeman, B., Needham, D.T., 1997. Quantitative fault seal prediction. AAPG Bull. 81, 897–917. https://doi.org/10.1306/522B498D-1727-11D7-8645000102C1865D.